Decarbonising the Glass Industry: A Comprehensive Techno-Economic Assessment of Low-Emission Pathways

Muhammad Salman[a]*, Daniel Flórez-Orrego[b], Diederik Coppitters[c], Rafailia Mitraki[a], François Maréchal[b], Grégoire Léonard[a]

[a] Chemical Engineering, University of Liège, Liège, Belgium

[b] IPESE group, Federal Polytechnic School of Lausanne, Sion, Switzerland

[c] Institute of Mechanics, Materials and Civil Engineering, Université Catholique de Louvain, Louvain-la-Neuve, Belgium

*Corresponding author: E-mail: m.salman@uliege.be

Abstract

The glass industry faces critical decarbonisation challenges due to high energy demand and reliance on fossil fuels. This study presents a comprehensive techno-economic analysis of diverse decarbonisation pathways for flat glass production, including electrification, energy efficiency, fuel switching and carbon capture and storage (CCS). A multi-scenario mapping explores sensitivity to future energy and carbon prices, while uncertainty quantification (UQ) assesses economic resilience under market volatility. From the results, a hybrid furnace (Hybfur), combining oxy-combustion and partial electrification, reduces emissions by 33% compared to conventional gas-fired furnaces (NGfur). All-electric (ELfur) and hydrogen-fired (H2fur) furnaces reduce emissions by 41% and 50%, respectively, eliminating combustion emissions. CCS achieves 50–74% emissions reductions, with a 5–22% energy demand increase. While NGfur remains cost-effective today, it faces a 57% total annual cost (TAC) increase in the 2050 scenario (scenario with high-carbon & low-renewable prices). Integrating CCS, though cost-intensive today, moderates the TAC increase in 2050. Hybfur achieves 40% and 20% lower TAC with and without CCS, respectively, compared to NGfur. ELfur, though currently expensive, achieves a 25% TAC reduction by 2050. Multi-scenario mapping shows that hybrid and oxy-fuel CCS configurations dominate across a wide range of future price conditions, whereas full electrification and hydrogen pathways require significant energy price reductions to become viable. Uncertainty analysis confirms that hybrid configurations maintain the highest probability of economic competitiveness under evolving market conditions. These findings highlight partial electrification as a key decarbonisation strategy, with CCS essential for deep emissions cuts and economic resilience under stringent climate policies.

Keywords: Glass industry, industrial decarbonisation, techno-economic analysis, electrification, carbon capture and storage (CCS), industrial energy transition, scenario-based analysis.

1. Introduction

Rising CO_2 levels pose a global threat, intensifying extreme weather and socio-economic risks (European Commission, 2023). Decarbonising the industrial sector is complex due to its high energy use, capital intensity and strict quality standards, especially in key sectors like steel, cement and glass (Bataille et al., 2018; Napp et al., 2014). Yet, their economic importance demands cost-effective, feasible solutions. The glass industry is a major source of industrial CO_2 emissions, contributing about 15 $MtCO_2$ annually in Europe (ETS, 2023a), with flat and container glass leading production. In Belgium, it emits 0.6 $MtCO_2$ per year, 78% of which is from flat glass (ETS, 2023b). The melting process, requiring temperatures of 1400–1650 °C (Joint Research Centre, 2013), entails high energy demand and offers limited decarbonisation alternatives. The strong dependency of the glass industry on natural gas (NG) emphasises the need for low-emission alternatives.

The flat glass industry has made significant progress in reducing emissions through improvements in furnace design, increased use of cullet (recycled glass) and enhanced energy efficiency (raw material preheating). As a result, emissions in the European flat glass industry decreased by 43% between 1990 and 2018 (Glass for Europe, 2020a). Although further refinements to the float process may yield slight efficiency gains, these rely on advanced technologies. Best available technologies and incremental improvements will continue to reduce emissions, but achieving climate neutrality by 2050 will require transformative measures like waste heat recovery, electrification, fuel switching and carbon capture and storage (CCS) (British Glass, 2021; Colangelo, 2024; Glass for Europe, 2020a; Griffin et al., 2021). These strategies could reduce emissions by 75–85% compared to 2018 levels (Glass for Europe, 2020a).

Recently, industries, researchers and governments have increasingly focused on exploring extensive decarbonisation options and technologies for flat glass production. A recent review of glass industry decarbonisation by Zier et al. (2021) identified key decarbonisation strategies, including electric melting, hydrogen combustion, waste heat recovery and process intensification. From the study, hybrid and all-electric melting, along with hydrogen oxy-fuel combustion, are promising, but they require further research, cost reductions and infrastructure adjustments. The study also emphasised advanced process controls, furnace efficiency and effective waste heat utilisation, while highlighting the need for lower renewable energy prices and robust infrastructure to enable the energy transition of the sector. Another study conducted by Zier et al. (2023) utilised a bottom-up model to assess CO_2 emissions and the impact of various decarbonisation options from 2020 to 2050 on the German container and flat glass industries. The study revealed that none of the modelled pathways are compatible with the strict 1.5 °C carbon budget, with even the best-case scenario exceeding it by +200%. Indeed, even the 2 °C target is reportedly feasible only through a complete fuel switch to green hydrogen or renewable electricity. The study also highlighted the significant CO_2 reduction potential of green hydrogen and stressed the importance of process-related emissions reductions, such as increasing cullet use, adopting alternative raw materials, or implementing CCS technologies. Papadogeorgos and Schure (2019) analysed decarbonisation options for the Dutch container and tableware glass industry, identifying key strategies, such as transitioning to all-electric furnaces, hydrogen combustion and using biomethane to replace NG. They emphasised the importance of increased cullet recycling to lower energy demand and emissions, as well as the potential of residual heat utilisation and CCS technologies. While these measures could significantly reduce emissions, their implementation requires further technological development, infrastructure upgrades and strong policy support, including carbon pricing and incentives for renewable energy. Barón et al. (2023) presented another perspective on the potential of decarbonisation along with the utilisation of captured CO_2. Their study presented a comprehensive analysis of Power-to-Gas (P2G) integration in the glassmaking industry. By combining CO_2 captured via Calcium Looping and green hydrogen from proton exchange membrane (PEM) electrolysers, synthetic natural gas replaces fossil NG in a closed-loop system. The proposed solution achieves up to 95% NG savings and 86% CO_2 emissions reduction with energy penalties of 32–35 GJ/t_{CO2}. Although the calculated carbon abatement costs (261–367 €/tCO_2) are relatively high, future scenarios with increased carbon taxes and renewable energy deployment may arguably enhance economic feasibility.

Although the studies mentioned above provide valuable insights into decarbonisation options, several critical gaps remain unaddressed. Most previous research focuses on individual technologies or strategies, lacking a systemic techno-economic analysis (TEA) that compares different decarbonisation pathways in terms of capital expenditures, operating expenses and energy consumption. Additionally, the potential of waste heat utilisation for carbon capture remains underexplored. Another key gap is the limited research on the impact of energy prices on the performance and economic feasibility of the system, particularly in the context of future energy scenarios. Recognising the conditions under which certain decarbonisation options become viable is crucial in aligning the configuration selection with future energy policies. Energy and carbon prices are subject to future uncertainties, making deterministic assessments insufficient. A robust analysis is needed to assess how variable energy prices and carbon taxes affect the suitability and ranking of various pathways over time.

Addressing these gaps is essential for identifying decarbonisation strategies that align with emissions reduction targets, such as the Fit-for-55 framework (European Commission, 2021) and the 2050 long-term strategy (European Commission, 2018). In this study, a bottom-up approach to analyse decarbonisation pathways in the glass industry is performed, focusing on detailed process-level modelling of key systems, including melting furnaces, energy systems and decarbonisation options. The options examined include electrification (all-electric and Hybrid (electric boosting) furnaces), hydrogen fuel switching, waste heat recovery and CCS. This study evaluates the tradeoff between the overall performance indicators, such as capital expenditures, operating expenses, energy consumption and CO_2 emissions. A multi-scenario mapping based on parameter sweep explores various decarbonisation options across a complex solution space. This approach identifies the conditions under which specific configurations/options are most viable and assesses their behaviour under various future energy scenarios. Lastly, to account for uncertainties in commodities and CO_2 emission prices, this study applies Uncertainty Quantification (UQ) in which Polynomial Chaos Expansion (PCE) is used as a surrogate-assisted UQ method, ensuring an efficient and reliable analysis with reduced computational cost. Hence, this study offers a robust framework for comparing decarbonisation options, assessing their technical and economic resilience, and providing policymakers and industry stakeholders with valuable insights to support cost-effective, energy-efficient strategies for deep decarbonisation of the glass industry. Its broader goal is to feed into the development of INDECATE (indecate.com), a web-based tool designed to aid decarbonisation decisions across sectors like glass, cement, steel, fertilisers, lime, and others.

2. Methodology

This bottom-up techno-economic assessment (TEA) of decarbonisation options for the glass industry follows four parts: data collection, model development, analysis and optimisation, and reporting (Figure 1).

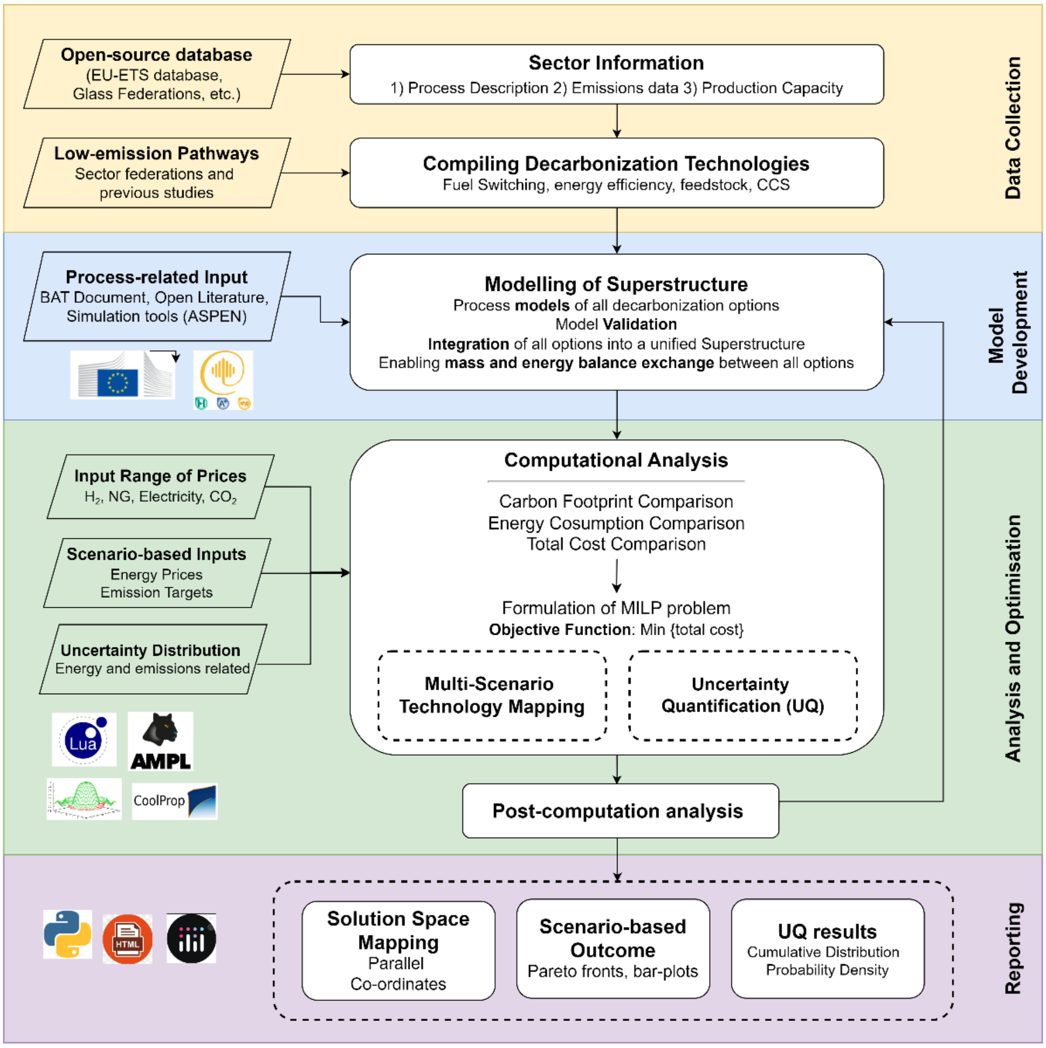

Figure 1. Comprehensive framework used to design and analyse decarbonisation pathways for glass production.

Data is sourced from open databases (e.g., EU-ETS (ETS, 2023b), (Glass for Europe, 2020a)), including process descriptions, emissions, and production capacities. Existing studies are reviewed to identify low-emission pathways. In the model development part, a superstructure integrates multiple decarbonisation options using data from the Best Available Techniques (BAT) document (Joint Research Centre, 2013) and simulation tools like Aspen Plus®. Validated models ensure mass and energy balances across equipment (Cervo et al., 2020). The analysis and optimisation evaluate energy use and economic performance across configurations. A multi-scenario parameter sweep identifies cost-effective pathways under diverse energy market conditions, while UQ assesses how energy price variability influences decarbonisation choices. The reporting part delivers insights to support informed decision-making. The methodology developed in this study (Figure 1) builds upon our previous work (Flórez-Orrego et al., 2022), with further improvements and extensions to include the parameter sweep method and the uncertainty quantification.

2.1 Modelling of the superstructure (description of the process, decarbonisation options and utility units)

A comprehensive set of decarbonisation options (Figure 2) is modelled using the equation-oriented or sequential modular simulation approaches. These models include mass and energy balance equations, CO_2 emissions data, costing parameters and other process design variables, rigorously validated against the literature to ensure accuracy. These ex-ante models are the foundation of the process synthesis and optimisation framework called OSMOSE Lua (Flórez-Orrego et al., 2022), which solves a mixed-integer linear programming (MILP) problem using the AMPL suite to identify the most cost-effective operating conditions and technologies for decarbonising the industrial sectors.

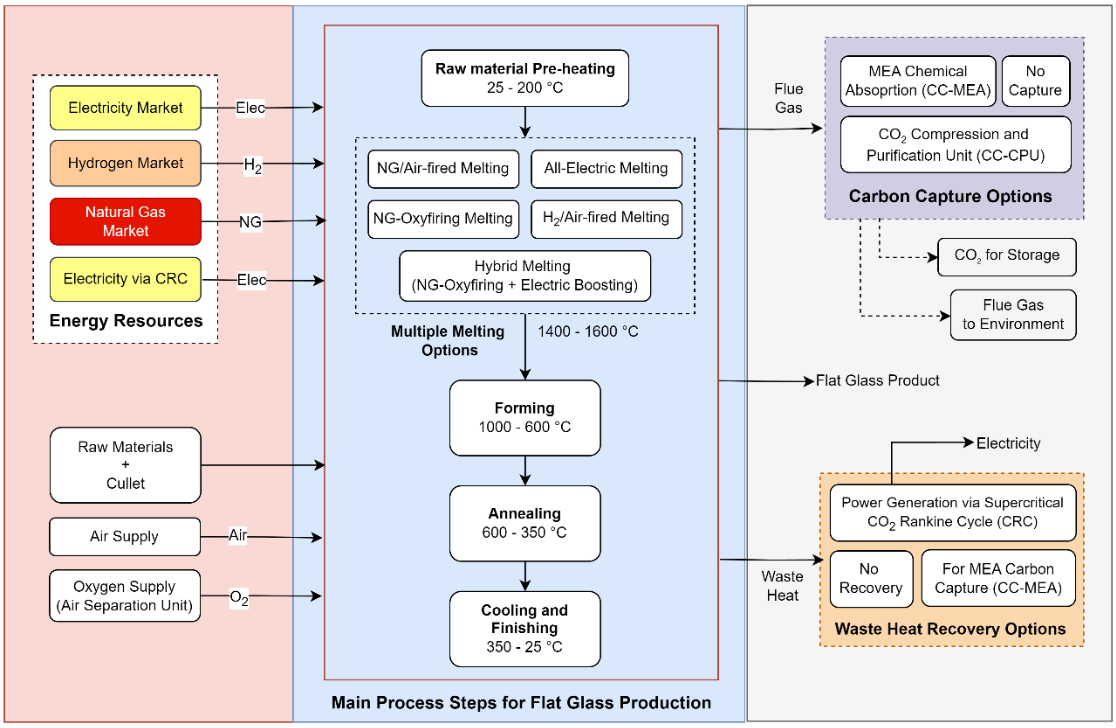

Figure 2. Superstructure of flat glass production incorporating a comprehensive set of options of energy resources, melting processes, CCS units and waste heat recovery methods.

This study considers a flat glass production plant with a capacity of 800 tonnes per day (tpd). Although flat and container glass serve different applications, their production processes share key similarities regarding melting technologies, furnace design, and energy efficiency strategies (B. Fleischmann, 2018; Joint Research Centre, 2013). Therefore, this study focuses only on the analysis of flat glass production to provide insights applicable to the broader glass sector. The process begins with batch preparation, where silica sand, soda ash, sodium sulfate, limestone, dolomite and cullet (recycled glass) are mixed and preheated to 200 °C using flue gas waste heat (Joint Research Centre, 2013). The batch is then melted at 1400–1600 °C in furnaces. In this work, various melting technologies and fuels are considered, as illustrated in Figure 2, including an air-gas furnace using NG or hydrogen as fuel (Joint Research Centre, 2013); an oxy-fuel furnace using NG as fuel; a hybrid furnace (combination of oxy-firing with 50% electric boosting); and an all-electric cold-top melting furnace. The OSMOSE Lua framework enables technology selection based on energy prices and emissions reduction goals. During melting, CO_2 is emitted from both fuel combustion and raw material decarbonation. The molten glass undergoes refining at 1300–1400 °C, followed by sheet formation in a tin float bath and gradual cooling in an annealing lehr (Joint Research Centre, 2013). A detailed process description and a flow diagram (courtesy of Glass for Europe (2020b)) are provided in supporting information Section S1. Operating parameters of a typical European facility, used in this study, are given in Table 1.

Table 1. Design parameters of a typical European flat glass production plant (Ecofys et al., 2012; Joint Research Centre, 2013)

Parameter	Value
Size	800 tpd (33 333 kg/h)
Raw Materials	1.15 t of solid mass/t of glass melted
Fuel	Natural gas (NG)
Fuel Consumption	49 MW (5.34 GJ/t_{glass})
Power Consumption	7.4 MW (0.8 GJ/t_{glass})
Emissions (Direct)	0.48 t_{CO2}/t_{glass}
CO_2 Concentration	8 – 16% mol.

To mitigate emissions, two carbon capture options are assessed. The first is chemical absorption using monoethanolamine (CC-MEA), where CO_2 is selectively absorbed from flue gas (40 °C) in an absorber, producing a CO_2-rich solvent. This is regenerated in a stripper at 120 °C using steam, releasing purified CO_2, which is then compressed for transport and storage, while lean MEA is recycled. The process is modelled in Aspen Plus® and integrated into OSMOSE. Detailed process description, operating parameters and a schematic diagram (Figure S2) of CC-MEA are provided in supporting information in section S2.1. Further design details can be found elsewhere (Salman et al., 2024).

The second carbon capture option is cryogenic CO_2 compression and purification (CC-CPU), used for flue gases from oxy-fuel and electric furnaces, which are rich in CO_2. After cooling and impurity removal, the gas is compressed to 25 bar, dried to 1 ppm moisture and sent to a cold box where CO_2 is separated from inerts. Depending on purity targets, multi-stage distillation or cold box configurations (as in the case of this study) can be applied. The regasified CO_2 is compressed for transport and storage (Shah, 2011). Energy, mass balances and cost data are taken from (Costa et al., 2024; Gardarsdottir et al., 2019; Shah, 2011). The detailed process description, operating parameters and a schematic diagram (Figure S3) of CC-CPU are provided in supporting information in section S2.2.

To draw a comparison between CC-MEA and CC-CPU, flue gases from air-blown furnaces are directed to CC-MEA and high CO_2 concentration streams from oxy-fired and all-electric systems are directed to CC-CPU, since cryogenic capture is generally employed in settings with high concentration oxy-combustion flue gases (Barlow et al., 2023). Both capture technologies include a compression train, compressing CO_2 up to 40 bar with a purity of 95% mol, aligning with the suggested Belgian CO_2 transport network requirement (Fluxys, 2022).

Two main external waste heat recovery approaches, namely, the electricity generation and the steam generation for amine solvent regeneration, are assessed. The flue gas from the furnace, after air preheating, serves as a heat source for a supercritical CO_2 Rankine cycle (CRC) (Figure S4). This cycle is more compact than conventional steam-based systems, benefiting from the higher density and operating pressures of CO_2 (>70 bar). It also uses superior heat transfer properties of supercritical fluid and a gliding evaporation temperature profile exceeding 300 °C, which aligns well with the hot air initial and final temperatures (400-600 °C) (Flórez-Orrego et al., 2023). This power cycle is modelled using the thermodynamic database CoolProp (CoolProp, 2023) and an equation-oriented simulation approach to optimise its performance and integration. The second integration route uses waste heat to generate steam (~120–150 °C) for the CC-MEA stripper reboiler, reducing external energy demand and auxiliary consumption while minimising waste heat rejection.

Table 2 summarises a list of the potential decarbonisation configurations (along with the abbreviations which are used throughout the paper) combining five primary melting furnace options, namely NG air-blown, NG-oxy-fired, Hybrid, Hydrogen air-blown and All-electric furnaces. Each furnace configuration can include or exclude carbon capture (-CC), resulting in a total of ten possible configurations. The oxyfiring configurations also include an air separation unit (ASU) for oxygen generation (description and operating parameters are given in the supporting information section S4). In addition, external waste heat recovery is implemented across all the configurations.

Table 2. Selected decarbonisation configurations for flat glass production.

Configuration	Abbreviation
NG air-blown furnace w/o CC (base case)	NGfur
NG air-blown furnace w/ CC	NGfur-CC
NG oxy-fuel furnace w/o CC	NGOxyfur
NG oxy-fuel furnace w/ CC	NGOxyfur-CC
Hybrid furnace (NG-oxy + 50% Electric boosting) w/o CC	Hybfur
Hybrid furnace (NG-oxy + 50% Electric boosting) w/ CC	Hybfur-CC
All-electric furnace w/o CC	ELfur
All-electric furnace w/ CC	ELfur-CC
H_2-air-blown furnace w/o CC	H2fur
H_2-air-blown furnace w/ CC	H2fur-CC

2.2: Emissions and Energy Performance Indicators

This section defines the performance indicators used to evaluate and compare decarbonisation configurations in terms of their emissions and energy intensities. It considers both the total CO_2 emissions and total energy demand (thermal and electrical) per tonne of flat glass produced, associated with each configuration. These indicators provide a consistent basis to assess the effectiveness of energy efficiency measures, fuel switching, electrification, and carbon capture strategies. The indicators are evaluated for each configuration using detailed process modelling and heat integration analysis, enabling a transparent comparison of energy use and environmental impact.

2.2.1 Carbon Footprint Calculation

To assess the CO_2 impact of each configuration, a carbon footprint analysis is performed, covering direct emissions from combustion and raw material decomposition (Scope 1), and indirect emissions from electricity and fuel supply chain (Scope 2).

Direct CO_2 emissions from NG combustion are calculated based on the thermal energy demand and the lower heating value of NG (50 MJ/kg). The fuel mass flow rate is determined, and CO_2 emissions are derived using stoichiometry, while considering furnace efficiency. Process-related CO_2 emissions stem from the decomposition of carbonate-based raw materials, such as sodium carbonate (Na_2CO_3), calcium carbonate ($CaCO_3$) and dolomite ($CaMg(CO_3)_2$). The emissions are quantified using stoichiometric emission factors based on molecular weights: 0.415 kg CO_2/kg Na_2CO_3, 0.44 kg CO_2/kg $CaCO_3$, and 0.477 kg CO_2/kg $CaMg(CO_3)_2$. These are multiplied by the corresponding mass flow rates of each material per tonne of glass to calculate the raw material-based direct emissions.

Indirect emissions are included to account for the upstream energy-related impact. A factor of 69 gCO_2/kWh (DG-Energy European Commission, 2015) is used for NG, based on its supply chain CO_2 emissions. For electricity and hydrogen, emission factors vary depending on the energy scenario. In the 2025 scenario, electricity is assumed to be predominantly fossil-based, with an indirect emissions factor of 145 gCO_2/kWh (EEA, 2024). For the 2050 scenario, a lower factor of 44 gCO_2/kWh_e (Frischknecht and Krebs, 2021; Schlömer et al., 2014) is applied, reflecting a shift to renewable electricity. In the 2025 scenario, hydrogen is assumed to be produced via steam methane reforming with CCS (blue hydrogen), with an emission factor of 87 gCO_2/kWh (IEA, 2023). For the 2050 scenario, 44 gCO_2/kWh is used, reflecting production through water electrolysis powered by renewable electricity (green hydrogen).

This carbon footprint calculation offers a simplified representative impact of the operational phase and supports the evaluation of the decarbonisation potential. A full life cycle assessment (LCA) is beyond the scope of this study.

2.2.2 Energy Consumption Analysis

This section outlines two key performance indicators: waste heat recovery potential and total specific energy consumption. Waste heat recovery identifies opportunities to reuse excess thermal energy, enhancing process efficiency and reducing external energy demand. Specific energy consumption quantifies the total energy (thermal and electrical) required per tonne of glass, considering both direct use and savings from recovery systems.

Energy efficiency is assessed using the pinch analysis method implemented in the OSMOSE Lua platform, which evaluates waste heat availability and its allocation to solvent regeneration (CC-MEA) or electricity generation (CRC). Two main waste heat sources are considered:

1) High-temperature flue gases exiting the furnace at 1300–1400 °C, which are used internally to preheat oxidants and raw materials, with residual heat available for external recovery at approximately 600 °C, assuming no air infiltration is done at the stack.
2) Glass annealing and cooling from 650 °C to 350 °C yields hot air at 200 °C available for recovery.

The optimisation framework ensures the physical constraint imposed by the minimum temperature difference (ΔT_{min}) between hot and cold streams. Equation (1) determines the amount of waste heat available after the regeneration and raw material preheating is discounted:

$$Q_{waste_i} = \left(Q_{melting} \cdot \left(1 - \eta_{fur_i}\right)\right) - \left(\frac{Q_{preheating,oxidant_i} + Q_{preheating,RM}}{\eta_{losses_i}}\right) - Q_{wall\ losses_i} + Q_{cooling} \quad (1)$$

where Q_{waste_i} is total waste heat (in MW) available for external recovery in the i^{th} configuration, η_{fur_i} is the efficiency of i^{th} furnace, $Q_{melting}$ is the total theoretical heat required for melting, $Q_{preheating,oxidant_i}$ is the theoretical heat required for preheating of air or oxygen, η_{losses_i} represents preheating losses (~10%), $Q_{preheating,RM}$ represents the preheating required by raw materials, $Q_{cooling}$ represent the waste heat recovered via glass cooling and $Q_{wall\,losses}$ is the heat lost through furnace walls.

The total specific energy consumption Q_{T_i} is evaluated using Equation 2, which accounts not only for the total energy demand but also for potential heat recovery opportunities within each configuration:

$$\frac{Q_{T_i}}{tonne\ of\ glass} = \frac{\left[\sum_{u \in units}(Q_u + P_u)\right] - Q_{rec} - P_{CRC}}{tonne\ of\ glass} \quad (2)$$

where, Q_u refers to the thermal energy demand P_u denotes the electric power required by each unit u. Meanwhile, Q_{rec} is the energy recovered through heat integration (for instance, for driving the CC) unit and P_{CRC} is the power generated by the waste heat recovery CRC for each configuration.

2.3 Economic analysis

The economic analysis comprises the total annual cost (TAC), the annualised capital expenditure (CAPEX) and operating expenditures (OPEX). Obtaining vendor quotes requires detailed equipment sizing and costly design decisions. Consequently, an engineering cost estimation method (Turton et al., 2018) that employs empirical correlations, estimation charts and correction factors to provide reliable cost estimates is implemented. The underlying principles and specific assumptions used in this analysis are outlined below.

2.3.1 Capital expenditures (CAPEX)

The CAPEX considers not only the equipment cost but also expenses owing to the installation, civil or engineering activities. Equation 3 calculates the total annualised CAPEX of each configuration.

$$Ann.CAPEX_i = \sum_{u \in units} \left[\left(CAPEX(u_{ref}) \cdot \left(\frac{S_0}{S_{ref}} \right)^{0.6} \cdot C_{BM} \cdot \frac{CEPCI_{2025}}{CEPCI_{ref}} \right) \cdot \frac{d \cdot (d+1)^n}{(d+1)^n - 1} \right] / \left(\frac{t_{glass}}{year} \right) \quad (3)$$

where, $Ann.CAPEX_i$ (€/t_{glass}) is the specific annual CAPEX of the i_{th} configuration, u stands for unit, S is the sizing factor of a given unit (e.g., glass production rate in case of furnace and CO_2 capture volume in case of CO_2 capture units), *ref* is the reference unit for calculations, and C_{BM} is the bare module cost factor encompassing direct and indirect expenses. Moreover, CAPEX is updated to 2025 values using the Chemical Engineering Plant Cost Index (CEPCI), with 2001 as the reference year, to account for inflation and market changes. The discount rate (d) and lifetime (n) are adjusted based on the type of unit used in each configuration.

Estimating the CAPEX of furnaces is challenging due to limited data availability and confidentiality concerns. Therefore, an alternative approach is adopted by splitting the CAPEX into burner (melting) system costs and fixed costs for other furnace components (e.g., forming, annealing, cooling and finishing). According to Blackburn (2016), the CAPEX for a flat glass production facility with a capacity of 500 tpd is estimated at €162 million. Assuming that the burner system accounts for approximately 30% of the total investment, the CAPEX attributable to the remaining plant infrastructure is €113.4 million. In this study, the total CAPEX for an 800 tpd facility is scaled accordingly using the CAPEX correlation presented in Equation (3). Furthermore, specific burner system costs are adopted from (Lyons et al., 2018), with values set at 236 €/kW for NGfur, 272 €/kW for H2fur, 225 €/kW for ELfur and 250 €/kW for NGOxyfur configurations. These values are applied consistently across the relevant furnace designs, ensuring a robust and technology-specific cost assessment framework. The cost of Hybfur is estimated as a 50% share of both electric and oxy-combustion furnaces. Hydrogen systems have higher CAPEX due to burner modifications and infrastructure upgrades. The electric furnaces feature the lowest CAPEX, as they avoid the regenerators and high-temperature crowns. Oxy-fuel systems slightly increase CAPEX due to the change in furnace type to a recuperator. This methodology ensures that only the incremental cost owing to fuel switching influences the CAPEX figures, while the remaining furnace cost remains unchanged across configurations.

Furnace lifetimes and discount rates are based on the BAT document (Joint Research Centre, 2013) and Technology Readiness Levels (TRL), with higher TRLs leading to lower discount rates and longer plant lifetimes. It can be explained by reduced risks and proven reliability. Lower TRLs entail higher discount rates and shorter lifetimes to account for uncertainties (Fujita, 2021). These factors are essential for assessing the feasibility of emerging decarbonisation technologies. Details on lifetimes, interest rates and TRLs are taken from multiple sources and compiled in Table 3 (Fuller et al., 2022; Joint Research Centre, 2013; Kobayashi, 2004; Morris, 2020; Rademaker and Marsidi, 2019; Zier et al., 2021).

Table 3. Technology readiness level, lifetime and discount rates are considered for each configuration.

Type	TRL (1-9)	Lifetime (years)	Discount rate (%)
NGfur	9	20	6
NGOxyfur	8 – 9	20	6
Hybfur	7 – 8	15	8
ELfur	6 – 7	10	8
H2fur	3 – 4	15	8

The flue gas composition and flow rate used to calculate the CAPEX of the CO_2 capture units are given in Table 4. For the CC-MEA unit, CAPEX includes all pre-operational costs, such as process engineering, equipment purchase, construction and installation. The simulation of the CC-MEA setup is developed in Aspen Plus®, whereas the previously described method is used to calculate the equipment costs as a function of various parameters, such as heat exchange area, column size, etc. Detailed CAPEX calculation steps are provided in our previous study (Kim and Léonard, 2025). The total specific $CAPEX(u_{ref})/S_{ref}$ from Equation 2 for the CC-MEA unit is 315 €/(tCO_2/y) in the case of NGfur and 420 €/(tCO_2/y) in the case of H2fur furnace. For the CC-CPU setup, the specific $CAPEX(u_{ref})/S_{ref}$ is reported by Gardarsdottir et al. (2019) as 148 €/(tCO_2/y) (S_{ref} = 0.87 $MtCO_2$/y).

The lifetime of the CO_2 capture units is set at 20 years, with a discount rate of 6%. CAPEX of both capture options contains the cost of capture and compression. For ASU $CAPEX(u_{ref})$ of €120 million is taken for the S_{ref} of 92 tonnes per hour (Air Liquide, 2020).

Table 4. CO_2 concentration and reference yearly CO_2 emissions for the different configurations when using a corresponding CO_2 capture Unit

Furnace type	mol% of CO_2 (wet basis)	$\boldsymbol{S_0}$ = Direct Emissions ($MtCO_2$/year)	CO_2 capture Unit
NGfur	8 – 16% (Joint Research Centre, 2013; Li et al., 2014)	0.14	CC-MEA
H2fur	6% (Calculated with Aspen Plus)	0.05	CC-MEA
NGOxyfur	40 – 50% (Kapoor and Schatz, 1997)	0.11	CC-CPU
Hybfur	60% (Calculated with Aspen Plus)	0.082	CC-CPU
ELfur	>60% (Assumed highly concentrated since only process emissions)	0.05	CC-CPU

For the CRC, the specific $CAPEX(u_{ref})/S_{ref}$ is based on the power generated by the CRC. In this study, the typical specific CAPEX of the supercritical CO_2 power cycle is around 1070 €/kW according to Wright and Anderson (2017). A lifetime of 20 years and a discount rate of 6% are considered.

2.3.2 Operating expenses (OPEX)

The OPEX (€/t_{glass}) encompasses fixed costs (e.g., labour, insurance and maintenance) and variable costs (e.g., electricity, steam, cooling water and raw materials) (Turton et al., 2018). Fixed operating costs are omitted to highlight the incremental OPEX. In this regard, variable costs associated with raw materials and utilities are included, considering the respective specific prices:

$$OPEX_i = \left(\left[\sum_{u \in units}\left(\sum_e\left(p_{e_u} \cdot \dot{Q}_{e_u}\right) + \left(p_{em_u} \cdot \dot{m}_{em_u}\right) + \sum_{RM}\left(p_{RM_u} \cdot \dot{m}_{RM_u}\right)\right) \cdot hrs\right] + \left(S_{CC} \cdot T\&S\ cost\right)\right) / \left(\frac{t_{glass}}{year}\right) \quad (4)$$

Where, $OPEX_i$ (€/t_{glass}) is the total specific OPEX of the i^{th} configuration, p is the specific price (€/unit), $\dot{Q}$ (kW) and $\dot{m}$ (kg/h) denote energy and mass flow rates, respectively, e refers to energy utilities (i.e., electricity, hydrogen and NG), em refers to emissions (i.e. CO_2), RM stands for raw materials, and hrs are the operating hours (8760 hours). The CO_2 transport and storage (T&S) costs are part of the OPEX and calculated on a per-tonne basis, based on the capture capacity (S_{CC}) in $MtCO_2$/year. The investment for T&S infrastructure is financed by enterprises developing and operating the networks, while industries pay only the cost of utilisation. In Belgium, the CO_2 T&S chain assumes onshore pipeline transport to the Zeebrugge terminal; offshore pipeline transport to North Sea storage sites; and final storage in saline aquifers or depleted gas fields (Fluxys, n.d.). The total T&S cost is estimated as 45 €/tCO_2. It includes both transport cost and storage cost, based on the work of Roussanaly et al. (2021). More details and assumptions for using the T&S cost calculation are provided in the Supporting Information Section S5.

Two operating scenarios are used to evaluate the OPEX of different configurations: (1) the 2025 Scenario, based on current market prices for electricity, NG, hydrogen and CO_2 emissions, sourced from market references; and (2) the 2050 Scenario (future outlook), which incorporates estimated prices from the PATHS2050 study by Vito (EnergyVille, 2023), including marginal production costs for energy commodities and projected CO_2 pricing. The aim is to assess the influence of future prices on the OPEX and the competitiveness of the various configurations. These prices are summarised in Table 5. The 2050 prices are marginal production costs based on assumptions and not actual price forecasts.

Table 5. Price scenarios and associated commodity prices. p_{EE} = electricity price, p_{NG} = NG price, p_{H2} = hydrogen price, p_{CO2} = CO_2 emissions price.

Scenario	Price	Value	Reference
2025	p_{EE}	78 (€/MWh)	(DG Energy, 2024a)
	p_{NG}	36 (€/MWh)	(DG Energy, 2024b)
	p_{H2}	120 (€/MWh)	(Business Analytiq, 2024)

	p_{CO2}	75 (€/t_{CO2})	(Statista, 2024)
2050	p_{EE}	56 (€/MWh)	(EnergyVille, 2023)
	p_{NG}	35 (€/MWh)	
	p_{H2}	78 (€/MWh)	
	p_{CO2}	250 (€/t_{CO2})	

2.3.3 Total annual cost (TAC)

The TAC (€/t_{glass}) represents the sum of annualised CAPEX and OPEX for each configuration. It provides an overall economic assessment, allowing for the comparison of different decarbonisation pathways under varying energy price conditions. TAC accounts for both investment and operational costs, evaluating the long-term feasibility of each configuration. Like OPEX, to evaluate TAC across different decarbonisation options, the same 2025 and 2050 scenarios described in the previous section are utilised. These scenarios reflect the current market conditions and the projected energy costs, enabling a comparative analysis of cost evolution over time. By evaluating these two scenarios, this study identifies which price variables have the greatest influence on each configuration and how shifting energy markets impact costs over time. However, its purpose is not at all to predict accurate flat glass production costs, but rather to provide a semi-quantitative comparison between technological choices.

2.4 Multi-scenario mapping of configurations (parameter sweep)

Following the TEA, a parameter sweep analysis is conducted to identify the most cost-effective decarbonisation pathways across a broad range of future energy and emission price scenarios. This approach moves beyond single-point forecasts by systematically varying key inputs, such as electricity, hydrogen, NG and CO_2 prices, reflecting uncertainties driven by policy changes, market volatility, infrastructure development, and geopolitical dynamics. The analysis reveals which configurations are most sensitive to pricing drivers and under what conditions they become economically viable. Technologies that only appear under extreme price scenarios suggest limited flexibility and heavy reliance on favourable but unlikely policy or market shifts, reducing their practical feasibility. In contrast, configurations that become viable under moderate variations in input prices indicate stronger economic robustness and adaptability, making them more suitable for future deployment in evolving energy systems.

To define the parameter ranges, data is sourced from Belgian and European energy distributors (ELIA, 2017; ENTSO, 2024, 2022) and research institutes (Climact, 2021; EnergyVille, 2023), which provide plausible projections for future energy prices and carbon costs. Based on these studies and energy scenarios, a broad range of energy commodities and CO_2 prices is considered. For instance, electricity prices range from as low as 10 €/MWh to as high as 200 €/MWh, covering the most plausible values to account for various possible scenarios. The same approach is applied to other commodity prices. The parameter space includes the following values:

$$\textit{Electricity Price } (p_{EE}) \left(\frac{€}{MWh}\right) \in [10, 25, 50, 75, 100, 125, 150, 175, 200]$$

$$\textit{Hydrogen Price } (p_{H2}) \left(\frac{€}{MWh}\right) \in [10, 25, 50, 75, 100, 150, 200]$$

$$\textit{NG Price } (p_{NG}) \left(\frac{€}{MWh}\right) \in [10, 35, 55, 75, 100]$$

$$\textit{CO}_2\textit{ Price } (p_{CO2}) (€/t) \in [75, 100, 150, 200, 250]$$

The parameter ranges are non-equidistant, the reason is to balance resolution and computational efficiency. Finer steps are used in low-price regions to capture sensitive shifts in competitiveness, while broader intervals at higher prices reflect regions where additional points add little value, as configurations consistently lose viability. This approach ensures focused insights with minimal redundant simulations. Next, the total number of parameter combinations is calculated based on the defined ranges:

$$N_{combinations} = | p_{EE} | \cdot | p_{H2} | \cdot | p_{NG} | \cdot | p_{CO2} | = 9 \cdot 7 \cdot 5 \cdot 5 = 1575 \; combinations \quad (4)$$

For each of these 1575 combinations of energy pricing scenarios, a MILP optimisation is executed to determine the most cost-effective configuration. The optimisation objective function is defined as:

$$Objective\,function = \min_i TAC_i = \min_i\,(Ann.CAPEX_i + OPEX_i) \quad (5)$$

Results are analysed using parallel coordinate plots, which provide an intuitive visualisation of the impact of different energy prices on the configuration selection. These plots compare the cost-effectiveness of technologies across scenarios, identify thresholds for which one configuration becomes more favourable and offer valuable insights into the competitiveness and suitability of decarbonisation technologies under varying conditions.

2.5 Uncertainty analysis (characterisation and quantification) related to the energy vector prices

The TAC of decarbonisation configurations is highly sensitive to energy vector and CO_2 prices. While the deterministic parameter sweep identifies cost-effective pathways, it does not reflect the probability of different scenarios occurring. To address this, Bayesian inference is applied, assigning lognormal priors to energy vectors and normal priors to CO_2 prices. Next, probable future values of the energy prices for 2030, 2040 and 2050 scenarios are obtained from studies conducted by Belgian and European energy distributors (ELIA, 2017; ENTSO, 2024, 2022) and research institutes (Climact, 2021; EnergyVille, 2023). The posterior distributions are estimated using a Markov Chain Monte Carlo (MCMC) method (Gefland & Smith, 1990), specifically the No-U-Turn Sampler (NUTS) (Hoffman and Gelman, 2014), a variant of Hamiltonian Monte Carlo (HMC). This approach leverages prior knowledge and observed data to model the uncertainty surrounding future energy and CO_2 emissions prices.

In this work, uncertainty in commodity price forecasts is assumed to increase with the time horizon due to factors like policy shifts, market volatility and technological change. Within the Bayesian framework, this is captured by assigning larger prior standard deviations and greater observational noise for later years. A total of 5,000 posterior samples are generated using MCMC (99% acceptance), with results shown in Figures S8 and S9. To propagate the input uncertainties through the model and quantify their effect on the quantities of interest, like TAC, PCE is adopted from the open-source Python framework RHEIA (Coppitters et al., 2022). For a detailed explanation of PCE, refer to Marelli and Sudret (2014). A brief description of the method is provided below. The PCE surrogate model ($\widehat{M}$) represents the input-output relationship of the system model (M) through a truncated series of multivariate orthonormal polynomials (Ψ), each scaled by corresponding coefficients (λ):

$$\widehat{M}_i(\xi) = \sum_{\{\alpha \in A_{\{\delta,\rho\}}\}} \lambda_{\{\alpha\}} \Psi_{\{\alpha\}}(\xi) \approx M_i(\xi) \quad (6)$$

where $\xi = (p_{EE}, p_{NG}, p_{H2}, p_{CO2})$ i.e., vector of independent random parameters, $i \in \{1,2,\ldots,10\}$ represents the configuration index, δ represents the number of uncertain input parameters, and α is a multi-index. The truncation reduces the series to $(\nu + 1)$ terms, determined by the polynomial order ρ and the number of uncertain parameters ($\delta = 4$). Here, $\nu + 1$ denotes the total number of multivariate polynomial terms retained in the truncated expansion, where ν is the number of coefficients excluding the constant. The order of the multivariate polynomial in the series corresponds to the sum of the orders of its univariate components (i.e., $|\alpha| = \rho$). Consequently, the multi-indices for polynomials of order ρ or lower are stored in the truncated set ($\mathcal{A}_{\delta,\rho}$) (Coppitters et al., 2020):

$$\mathcal{A}_{\delta,\rho} = \{\alpha \in \mathrm{N}^{\delta} : |\alpha| \leq \rho\} (7)$$

N represents the set of natural numbers. The number of multi-indices in ($\mathcal{A}_{\delta,\rho}$) is given by (Coppitters et al., 2020):

$$\mathrm{card}(\mathcal{A}_{\delta,\rho}) = \binom{\rho+\delta}{\rho} = \frac{(\delta+\rho)!}{\delta!\,\rho!} = \nu + 1 \quad (8)$$

The PCE coefficients λ are estimated using a regression-based approach (Coppitters et al., 2020). To ensure a well-posed least-squares minimisation, at least $2(\nu + 1)$ training samples are used. These are generated via quasi-random Sobol sampling and evaluated using the full system model M. A polynomial order of ρ = 3 results in 70 required samples, ensuring a Leave-One-Out (LOO) cross-validation error below 1% per PCE. Once constructed, PCEs enable analytical computation of statistical moments and sensitivity indices, while allowing efficient probability density function (PDF) reconstruction without further model evaluations. The process is repeated for each configuration across three target years (2030, 2040 and 2050), resulting in 30 PCE models.

3 Results and Discussion

This section presents the results of the proposed decarbonisation pathways, evaluated across a range of energy scenarios. The analysis begins with a detailed carbon footprint comparison to quantify the climate impact of each furnace configuration. This is followed by an energy performance assessment, highlighting waste heat recovery potential and specific energy demand, particularly in the context of carbon capture and power generation integration. An economic analysis sheds light on the impact of the energy and CO_2 prices and capital investment on the TAC of each configuration. Results of a multi-scenario mapping are explored, showing how variations in the prices influence the optimality of specific configurations, thus providing a clear understanding of the solution space. Finally, by considering uncertainties in the prices, the analysis determines which configurations are likely to be a cost-optimal solution.

3.1 Emissions and Energy Performance Indicators

This section presents two key performance aspects of the assessed configurations. First, the carbon footprint is evaluated by accounting for direct process and combustion emissions, as well as indirect emissions from electricity and the fuel supply chain. Next, the energy consumption is analysed to assess the specific energy demand and waste heat recovery potential of each configuration.

3.1.1 Carbon Footprint Calculation

The CO_2 emissions performance of the various configurations depends on choices about energy vectors and the inclusion of carbon capture units. The detailed emissions breakdown is shown in Figure 3. For the 2025 scenario, in which electricity and hydrogen are assumed fossil-derived, the NGfur configuration shows the highest CO_2 emissions ratios at 0.61 t_{CO2}/t_{glass}, driven by direct NG combustion emissions (0.29 t_{CO2}/t_{glass}), process emissions from the raw material decomposition (0.19 t_{CO2}/t_{glass}), and indirect/upstream emissions of NG (0.10 t_{CO2}/t_{glass}) and electricity (0.023 t_{CO2}/t_{glass}). Integrating CC-MEA (NGfur-CC) reduces the net emissions to 0.22 t_{CO2}/t_{glass}, leaving only unabated emissions (0.053 t_{CO2}/t_{glass}) due to CO_2 capture inefficiency and indirect emissions (0.16 t_{CO2}/t_{glass}).

NGOxyfur configuration shows modest improvement in terms of fuel savings, resulting in 11.5% lower emissions (0.54 t_{CO2}/t_{glass}) than NGfur. With carbon capture (NGOxyfur-CC), it achieves 0.16 t_{CO2}/t_{glass}, aided by capture via CC-CPU and reduced fuel use, though indirect emissions of NG supply still contribute 0.081 t_{CO2}/t_{glass}. Hybfur configuration benefits from partial electrification, reducing total emissions to 0.41 t_{CO2}/t_{glass}. Paired with carbon capture, Hybfur-CC reaches 0.15 t_{CO2}/t_{glass}, i.e. the lowest total emissions in the 2025 scenario. This emphasises the importance of combining electrification with CCS techniques.

Full electrification (ELfur) eliminates direct combustion-related emissions, resulting in a total of 0.36 t_{CO2}/t_{glass} (41% lower than in NGfur), attributable entirely to process emissions and indirect emissions from electricity use. With carbon capture (ELfur-CC), CO_2 emissions are further reduced (0.19 t_{CO2}/t_{glass}) by tackling process-related CO_2 and modest power-related emissions (0.18 t_{CO2}/t_{glass}). Hydrogen-fired furnaces result in similar CO_2 emissions profiles while eliminating the direct combustion CO_2 emissions. In the 2025 scenario, H2fur and H2fur-CC reach net emissions of 0.35 and 0.19 t_{CO2}/t_{glass}, respectively, due to zero combustion CO_2 emissions and process emissions cut down via CCS implementation. By 2050, with fully renewable electricity and hydrogen, indirect emissions drop sharply. ELfur-CC and H2fur-CC outperform with 0.06 and 0.09 t_{CO2}/t_{glass} total emissions, respectively, leveraging upstream decarbonisation. NG-based configurations see limited improvement in 2050.

As a result, CCS implementation is essential across all configurations to address process CO_2 emissions. Hybrid furnaces offer an effective transitional solution, with significant emissions reduction through partial electrification. Electrification and hydrogen become most effective at the same time that electricity grids and hydrogen supply chains are decarbonised.

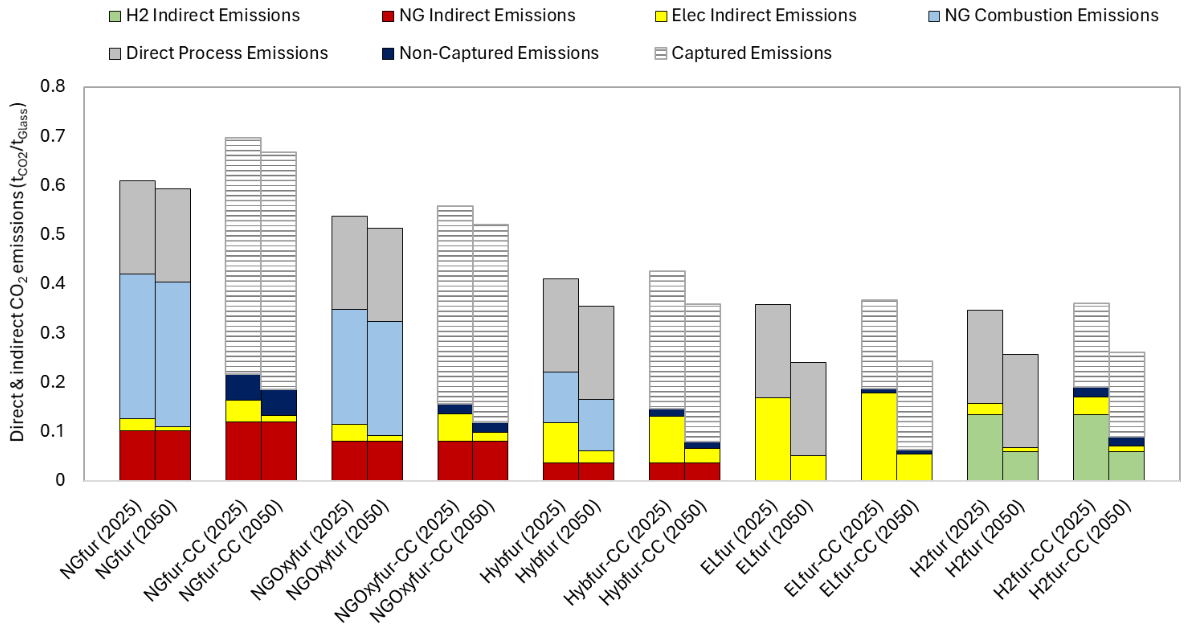

Figure 3. CO_2 emissions breakdown per tonne of glass across all configurations for 2025 and 2050 scenarios, including direct, indirect and process-related emissions. For CCS-based configurations, captured CO_2 emissions are shown with hatched bars to illustrate the total CO_2 generated and the portion effectively captured.

3.1.2 Waste heat recovery

Waste heat recovery analysis was conducted for each configuration, with results shown in Figures 4–6 and summarised in Table 6. The total available waste heat and its internal and external recovery are reported. Notably, in cases where CC-MEA is activated, CRC is not selected, as the available waste heat is prioritised for solvent regeneration, leaving insufficient heat for CRC.

Table 6. Waste heat recovery potential and resultant emissions reduction for all configurations.

Configuration	Total Waste heat available (MW)	Heat recovered for preheating, including losses (MW)	Heat Recovered for CC-MEA unit (MW)	Electricity generated via the CRC system (MW)
NGfur	17.4	10.6	-	2.0
NGfur-CC	17.4	10.6	6.1	-
NGOxyfur (-CC)	12	5	-	2.1
Hybfur (-CC)	7.46	2.9	-	1.36
H2fur	16.6	9.45	-	2.15
H2fur-CC	16.6	9.45	4.7	-
ELfur (-CC)	0	0	0	0

For the NGfur option, 14 MW of heat is recovered from exhaust gases and 3.4 MW from cooling at 200 °C. After allocating 9 MW to air (1200 °C) and 1.6 MW to raw material (200 °C) preheating, the remainder 6.8 MW (Q_{waste}) is utilised in a CRC system (450 °C) that generates 2.0 MW of electricity with an efficiency of 30%. This reduces auxiliary power demand by 27% (from 7.4 to 5.4 MW) and cuts indirect emissions by 2.5 $ktCO_2$/year, considering the grid emission intensity of 145 gCO_2/kWh_e (EEA, 2024). The integrated composite curve is shown in Figure 4(a). In the NGfur-CC case (Figure 4b), out of 17.4 MW, 6.1 MW (Q_{waste}) is used by the CC-MEA unit (at ~120 °C), with the remainder covering the preheating need. Carbon capture with amines requires 3.6 GJ/t_{CO2} (Salman et al., 2024), resulting in a total heat demand of 13.4 MW in this case. The remaining 7.3 MW heating demand is met using an auxiliary NG-fired boiler. This heat recovery results in reduces the energy demand of CC-MEA from 3.6 to 1.6 GJ/tCO_2 and results in an emission reduction of 4.3 ktCO_2/year as a result of fuel savings, assuming 85% boiler efficiency and 69 gCO_2/kWh indirect emission intensity of NG (DG-Energy European Commission, 2015).

In the NGOxyfur configuration, 12 MW of waste heat is recovered, 8.6 MW from exhaust gases (1400 °C) and 3.4 MW from forming cooling (200 °C). Prioritising high-temperature process streams, 3.4 MW is allocated for oxygen preheating (600 °C) and 1.6 MW for raw material preheating. The remaining 7.0 MW (Q_{waste}) powers a CRC system, generating 2.1 MW of electricity, reducing electricity import by 28% (from 7.4 MW to 5.3 MW) and avoiding 2.66 ktCO_2/year. Figure 5(a) shows the integrated composite curves. Although the NGOxyfur configuration produces less waste heat than the NGfur option, its lower preheating demand for oxygen also offsets this difference. The NGOxyfur-CC case involves higher power demand due to added CC-CPU and ASU units. In comparison, Hybfur (Figure 5b) has lower NG combustion and waste heat but still generates 1.36 MW via CRC.

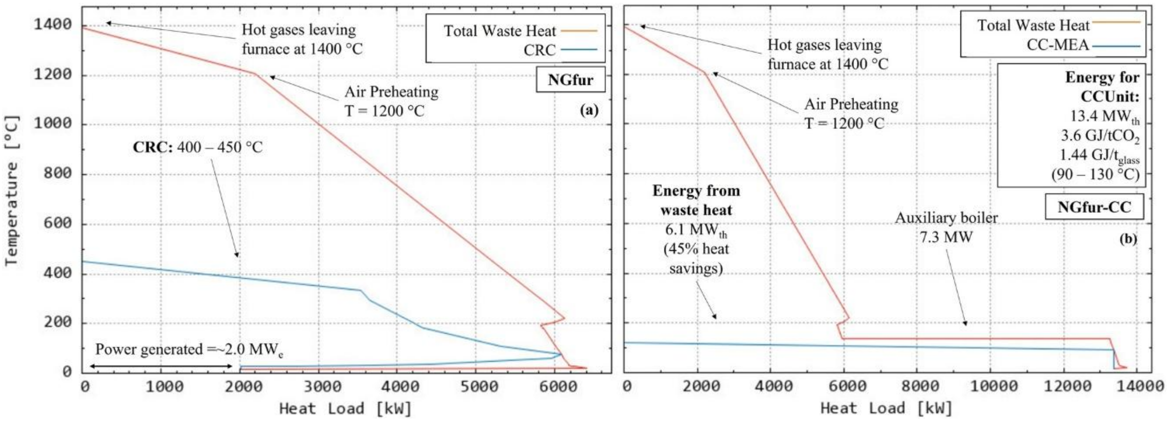

Figure 4. Integrated composite curves: (a) for NGfur configuration, recovering waste heat via CRC, (b) NGfur-CC configuration, recovering waste heat for CC-MEA unit.

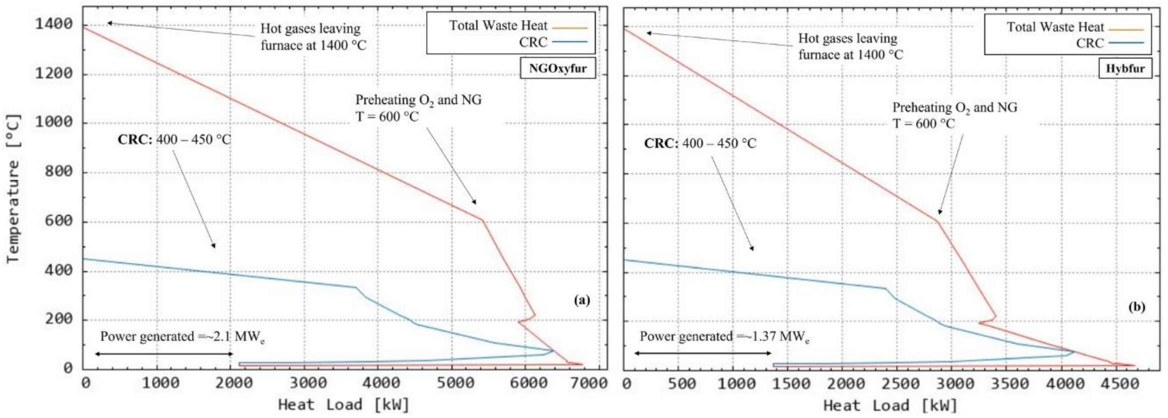

Figure 5. Integrated composite curves of (a) NGOxyfur configuration and (b) Hybfur configuration, highlighting the power generation potential using a CRC system.

Figures 6(a) and 6(b) illustrate the integrated composite curves for the H2fur and H2fur-CC configurations. In the H2fur setup, approximately 2.15 MW of electricity is generated through a CRC system, which reduces electricity purchase from the grid and avoids around 2.73 ktCO_2/year. In the H2fur (-CC) configurations, there are no combustion-related emissions. As a result, only 4.7 MW of heat is needed for the CC-MEA unit, which can be fully supplied using available waste heat, eliminating the need for an auxiliary boiler. This configuration shows how using a clean fuel like hydrogen can lower combustion emissions and reduce the energy demand of the capture system, allowing it to be fully supplied by waste heat and making the setup self-sufficient, preventing approximately 3.3 ktCO_2/year in terms of fuel savings. In contrast, the ELfur configuration lacks sufficient flue gas energy, limiting the effectiveness of waste heat recovery and preventing integration of the CRC system.

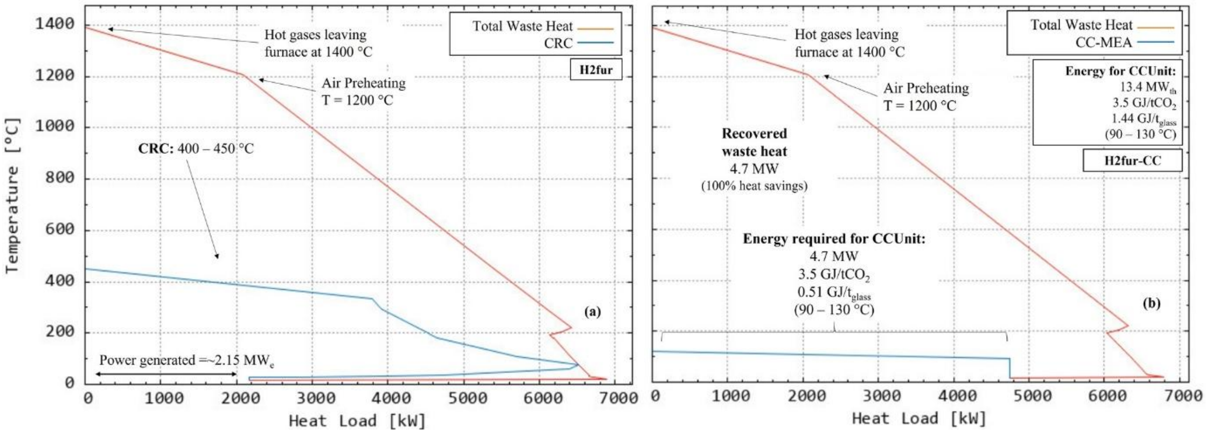

Figure 6. Integrated composite curves of (a) H2fur configuration recovering waste heat via CRC system and (b) H2fur-CC configuration recovering waste heat for CC-MEA unit.

3.1.3 Specific energy consumption

Figure 7 shows the energy breakdown (thermal and electrical demand, and heat recovery in GJ/t_{glass}) and total CO_2 emissions (direct and indirect) across all configurations.

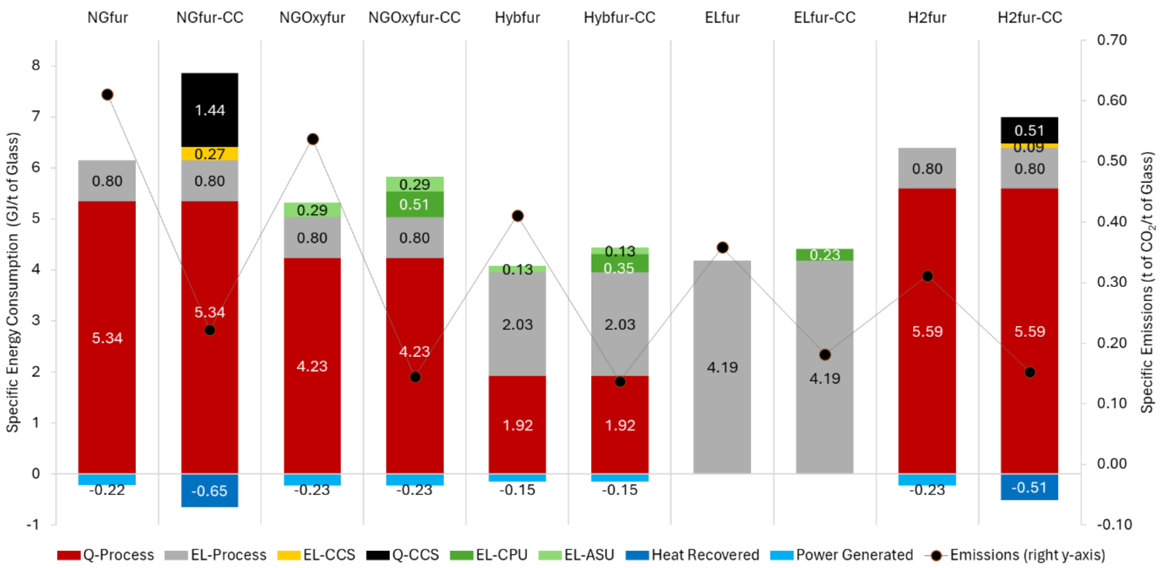

Figure 7. Energy consumption breakdown (left axis) and total CO_2 emissions (right axis) for all the studied configurations. Q-process and EL-process: heating demand and electricity consumption of the glass process; Q-CCS and EL-CCS: heating demand and electricity consumption of the CC-MEA unit; EL-CPU and EL-ASU: electricity consumption of the CC-CPU and the ASU of the oxy-combustion process; Heat and power recovered: avoided heating and electricity import via waste heat recovery.

In the base case (NGfur), the total energy demand is 5.92 GJ/t_{glass}, of which thermal demand is 5.34 GJ/t_{glass}, electrical demand is 0.58 GJ/t_{glass}, with emissions of 0.61 t_{CO2}/t_{glass}. Although total electrical demand is 0.8 GJ/t_{glass}, it is reduced to 0.58 GJ/t_{glass}, thanks to 0.22 GJ/t_{glass} power generated by CRC via waste heat recovery. Switching to NGOxyfur lowers energy demand to 5.1 GJ/t_{glass}, despite an increase in electrical consumption due to the addition of the ASU. Hybfur reduces total emissions by 33% and further lowers overall energy demand to 3.93 GJ/t_{glass}, although it results in a 2.5-fold increase in electricity consumption (2.03 GJ/t_{glass}). H2fur shows a slightly higher thermal demand but achieves lower emissions (0.31 t_{CO2}/t_{glass}) compared to NGfur. The ELfur configuration eliminates fuel use, requiring 4.19 GJ/t_{glass} of total energy. Emissions are entirely dependent on raw material decarbonation and the carbon intensity of the electricity grid, amounting to 0.36 t_{CO2}/t_{glass}. A direct comparison between NGfur and electric-based options (Hybfur and ELfur) reveals that electrification significantly cuts down the total energy demand due to higher efficiency, but it increases the reliance on green electricity availability.

Integrating CCS cuts emissions by 50–74% but increases energy demand. NGfur-CC reduces emissions by 64% but has the highest energy use (7.20 GJ/t_{glass}) due to additional heating for CO_2 capture. NGOxyfur-CC (5.6 GJ/t_{glass}), though having higher electricity demand for ASU and CC-CPU, is more efficient (0.14 t_{CO2}/t_{glass}), owing to higher capture efficiency and reduced flue gas volume. Hybfur-CC is the most energy-efficient carbon capture configuration (4.3 GJ/t_{glass}), minimising CCS penalties through lower fuel use. H2fur-CC (6.5 GJ/t_{glass}) is also more efficient than NGfur-CC due to lower combustion emissions, reducing MEA regeneration heat needs. Moreover, waste heat recovery supports CCS integration by supplying energy for MEA regeneration and electricity via CRC.

From an energy efficiency perspective, Hybfur is the most efficient non-CCS option, reducing NG use through partial electrification. It is closely followed by ELfur. NGOxyfur benefits from oxy-combustion, while H2fur, despite zero combustion emissions, has a slightly higher demand. Only ELfur eliminates external fuel use, though its performance depends on the carbon intensity of the grid. Among CCS configurations, Hybfur-CC and ELfur-CC are the most energy-efficient options and effectively minimise CCS-related penalties. NGfur-CC has the highest energy demand, while H2fur-CC improves efficiency by lowering capture-related heat needs. Overall, Hybfur and Hybfur-CC offer the best trade-off between efficiency and emissions reduction, although the ELfur configurations also perform quite similarly.

3.2 Economic feasibility analysis

The study of the economic feasibility of the different decarbonisation pathways for flat glass production considers the CAPEX and OPEX as elements of the TAC of each configuration. The former captures the impact of the required infrastructure investments on furnaces, carbon capture systems and waste heat recovery. Meanwhile, the OPEX reflects operational expenses, such as fuel, electricity, hydrogen, emissions allowances and T&S cost of captured CO_2. A cost analysis across two different scenarios sheds light on how shifting energy prices, adopting carbon taxes and promoting technological improvements influence the long-term competitiveness of the studied configurations.

3.2.1 Comparative analysis of the capital expenditures

According to Figure 8, furnace CAPEX ranges from 55 €/t_{glass} for the conventional NGfur configuration to 60 €/t_{glass} for the ELfur configuration. The slightly higher costs for ELfur (60 €/t_{glass}) and H2fur (59 €/t_{glass}) reflect the need for specialised equipment, such as electric boosters, high-temperature-resistant materials and advanced burner systems. Hybrid furnaces (58 €/t_{glass}) also exhibit marginally higher costs than the NGfur, due to the integration of electric boosting and oxy-fuel components, which increases system complexity.

As shown in Figure 8, the addition of carbon capture significantly raises the initial investment. For instance, NGfur-CC incurs an additional 11.3 €/t_{glass} over the base case, primarily due to the CC-MEA system, which includes absorption and stripping columns, heat exchangers and CO_2 compression. In contrast, CC-CPU adds 7.56 €/t_{glass} in NGOxyfur-CC, 5.26 €/t_{glass} in Hybfur-CC and 3.40 €/t_{glass} in ELfur-CC. CC-CPU is more compact and omits thermal amine regeneration, making it less capital-intensive. However, ASU costs must also be considered in CC-CPU-based options. NGOxyfur-CC and Hybfur-CC require an additional 4.89 €/t_{glass} and 2.19 €/t_{glass}, respectively, for ASU investment. This brings the total carbon capture CAPEX for NGOxyfur-CC to 12.45 €/t_{glass}, which is 9.2% higher than NGfur-CC. Despite added ASU costs, CC-CPU configurations benefit from lower thermal energy demand (cf. Section 3.1.2). In the case of H2fur-CC, the CC-MEA system results in an additional CAPEX of 3.91 €/t_{glass}, which is 65% lower than the CC-MEA CAPEX of the NGfur-CC configuration. This indicates that the decrease in capture size results in lower CAPEX per tonne of glass while eliminating combustion emissions.

The CRC system contributes modestly to CAPEX, ranging from 0.39 €/t_{glass} to 0.54 €/t_{glass} across configurations, reflecting the cost of heat exchangers, expanders and auxiliary components. Overall, fuel switching and electrification increase the furnace CAPEX by approximately 4% to 9%, reflecting the additional equipment and integration requirements. Implementing carbon capture systems incurs significantly higher capital costs, adding approximately 6% to 20% over the respective non-CC cases. H_2-fired systems with minimal capture needs offer another favourable balance between cost and emissions reduction.

Moreover, it is worth mentioning here, that these CAPEX figures assume a greenfield scenario (new build). In brownfield (retrofit) projects, integration complexity, equipment modifications and downtime would likely increase total investment costs.

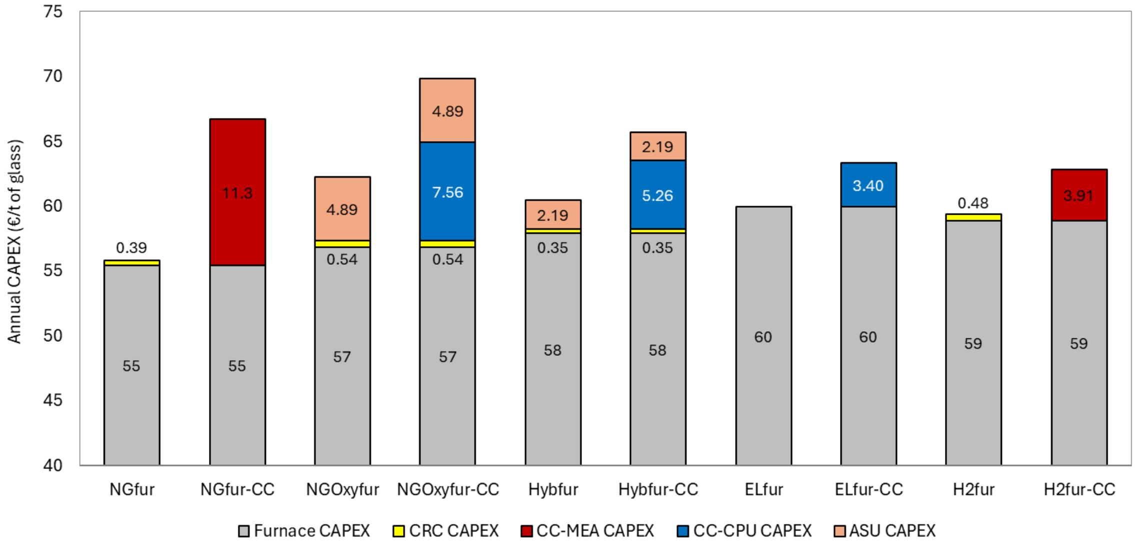

Figure 8. Breakdown of the annualised CAPEX of all the studied configurations (€/t_{glass}). Note: The y-axis of the graph starts from 40 €/t_{glass} to highlight the relative incremental burners and additional units' costs.

3.2.2 Comparative analysis of the operating expenditures

The breakdown of the OPEX under current and future carbon pricing and energy cost scenarios is shown in Figure 9. The furnace OPEX ranges from 181 €/t_{glass} for NGfur to 300 €/t_{glass} for H2fur under 2025 market conditions. NGOxyfur (177 €/t_{glass}) offers the lowest OPEX due to low NG and moderate CO_2 prices. It benefits from improved combustion efficiency but requires additional electricity for the ASU, slightly offsetting energy-saving gains. Hybfur (178 €/t_{glass}) remains competitive, with partial electrification reducing NG use and emission cost. In contrast, ELfur (214 €/t_{glass}) and H2fur (300 €/t_{glass}) exhibit higher OPEX due to high electricity and hydrogen prices.

In the 2050 scenario, with higher carbon and lower renewable energy prices, advanced configurations become more viable. NGfur and NGOxyfur see significant OPEX increases to 317 €/t_{glass} (+43%) and 289 €/t_{glass} (+40%), respectively, highlighting the vulnerability of fossil-based systems in carbon-constrained economies. Hybfur increases modestly to 239 €/t_{glass} (+25%), while ELfur remains relatively stable at 218 €/t_{glass} (+2%), demonstrating resilience under favourable renewable energy scenarios. Although H2fur benefits from hydrogen price reductions, its OPEX remains high at 283 €/t_{glass}, indicating a need for a significant decrease in hydrogen prices for it to be favourable.

Carbon capture integration (-CC) is initially costly in 2025 but offers economic benefits in 2050 (i.e., for high emission and low renewable prices scenario). In 2025, NGfur-CC (206 €/t_{glass}) adds 23 €/t_{glass} over NGfur, primarily due to CCS operating costs. Similar trends are seen for NGOxyfur-CC (186 €/t_{glass}), Hybfur-CC (185 €/t_{glass}) and ELfur-CC (218 €/t_{glass}), where CCS integration modestly increases OPEX. However, in 2050, NGfur-CC sees only a 2% OPEX increase (209 €/t_{glass}) versus a 43% increase for NGfur. Likewise, NGOxyfur-CC (171 €/t_{glass}) and Hybfur-CC (157 €/t_{glass}) outperform their non-CC counterparts. ELfur-CC (165 €/t_{glass}) also emerges as one of the most cost-effective options, second only to Hybfur-CC. Although H2fur-CC (236 €/t_{glass}) is not the lowest-cost option in terms of OPEX by 2050, it remains more economically viable than its non-CC counterpart.

Configurations without carbon capture units have an operating cost advantage in the current scenario of energy and CO_2 emissions prices. However, they become more expensive in 2050, rendering the configurations equipped with carbon capture technologies more viable. Nevertheless, given the uncertainty of future energy markets, a balanced approach is crucial for cost stability and emissions reduction.

Fossil fuel reliance without carbon capture is unsustainable under stringent carbon costing scenarios, whereas full electrification and hydrogen adoption depend on significant cost reductions in renewable electricity and power-to-gas systems. Hybrid furnaces (with or without carbon capture) provide a practical transition, as they simultaneously reduce emissions and ensure cost stability. Their compatibility with carbon capture technologies enhances the long-term viability, thus advancing glass industry decarbonisation with marginal risk from energy price volatility.

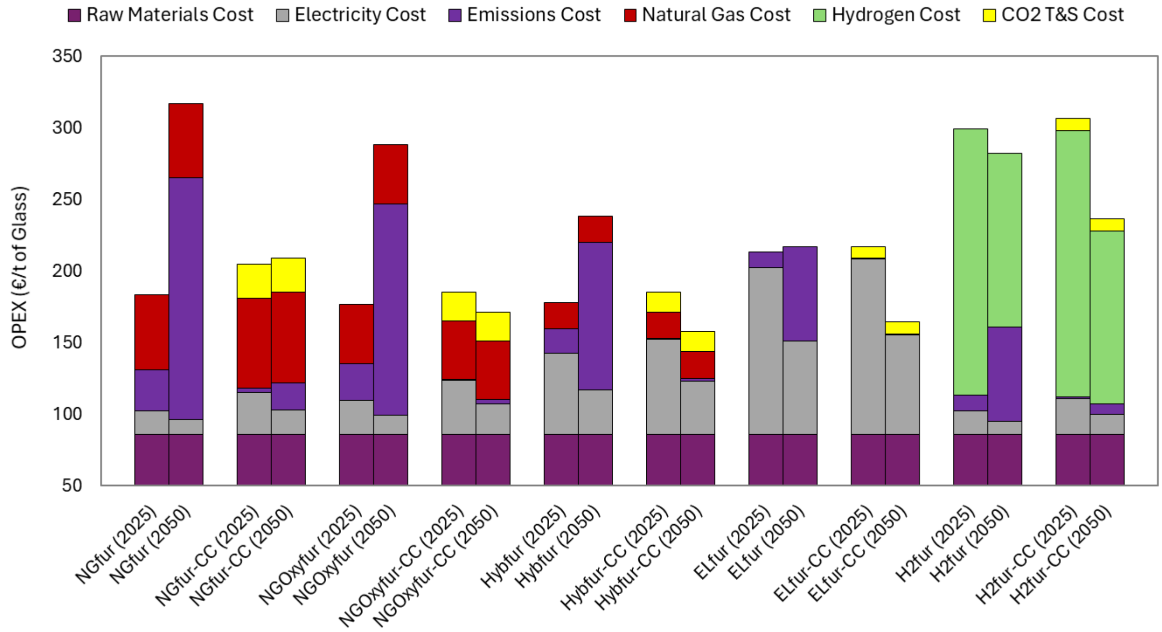

Figure 9. Breakdown of operational expenses (OPEX) for the studied configurations using commodity prices for 2025 and 2050. Note: The y-axis begins at 50 €/t to account for the constant cost of raw materials and to better emphasise the relative contribution of energy commodities.

3.2.3 Total annual cost estimation

The TAC reflects the overall impact of decarbonisation strategies under evolving energy and CO_2 pricing. A Pareto plot comparing TAC, CO_2 emissions (direct emissions + energy-related indirect emissions) and specific energy consumption is shown in Figure 10.

In the 2025 scenario, NGfur has the lowest TAC (237 €/t_{glass}), but this surges to 373 €/t_{glass} in the 2050 scenario due to rising carbon prices. While NGfur-CC reduces emissions, its 2025 TAC increases to 272 €/t_{glass}, making it economically unviable in the short term. However, in 2050, its TAC drops to 269 €/t_{glass}, below that of NGfur, revealing its potential to mitigate long-term CO_2 taxation risks despite limited efficiency gains compared to other decarbonisation options.

NGOxyfur shows higher efficiency than NGfur, with lower fuel use and a slightly reduced TAC in 2050 (351 €/t_{glass}) compared to the TAC of NGfur. When combined with carbon capture (NGOxyfur-CC), emissions drop significantly and the 2050 TAC decreases further to 241 €/t_{glass}, outperforming NGfur-CC. This highlights the advantage of oxy-combustion integrated with CC-CPU, especially under a higher carbon pricing scenario.

The Hybfur configuration integrates partial electrification, reducing NG dependence, energy consumption and environmental impact. Its TAC in 2025 (239 €/t_{glass}) is comparable to NGfur, but in 2050, it increases moderately to 299 €/t_{glass}, unlike NGfur, which increases more dramatically. Improved efficiency and lower CO_2 emissions make Hybfur the most cost-effective non-CC option in a high carbon price scenario. When paired with CO_2 capture (Hybfur-CC), emissions decrease further and TAC drops to 223 €/t_{glass} in 2050, positioning it among the most viable decarbonisation pathways. Although its 2025 cost aligns closely with NGfur, hybrid electrification outperforms NGfur under rising carbon prices and expanding access to cheap renewable electricity.

On the other hand, the ELfur configuration eliminates fossil fuel use and shows notable cost stability. Its TAC in 2025 (274 €/t_{glass}) is higher than NGfur, but in 2050, it becomes the lowest-cost option without carbon capture (278 €/t_{glass}), due to the absence of combustion emissions and lower electricity prices. The ELfur-CC configuration sees a significant TAC reduction from 281 €/t_{glass} in 2025 to 229 €/t_{glass} in 2050, making it more competitive than NGfur-CC. This suggests that, although electrification with carbon capture is currently expensive, it may become a viable option as renewable electricity prices decline.

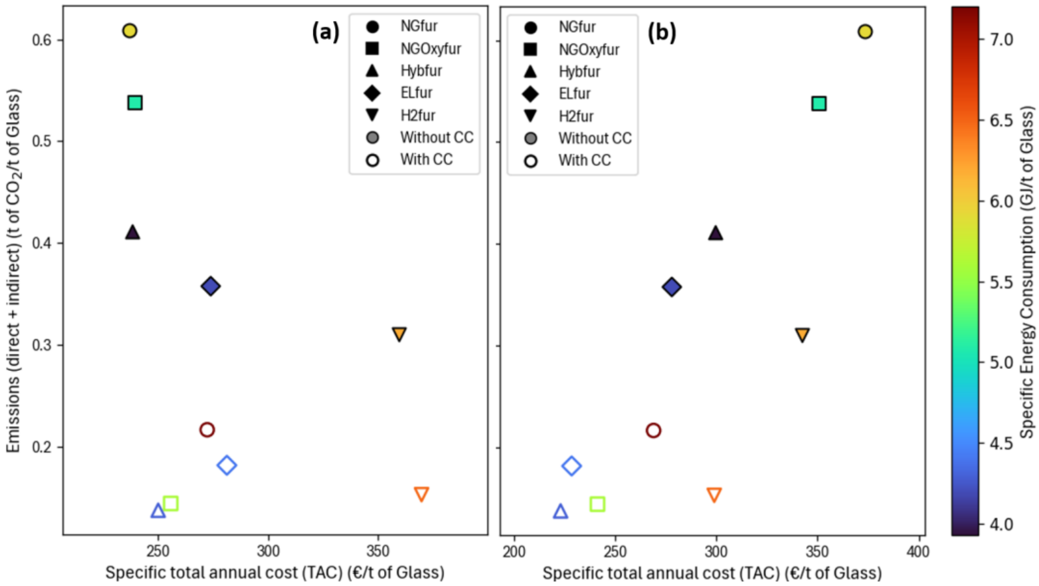

Figure 10. Pareto plots relating the TAC, CO_2 emissions and specific energy consumption of all the studied configurations for (a) 2025 (left) and (b) 2050 (right) scenarios.

The H2fur configuration remains the least cost-effective in 2025, with a TAC of 359 €/t_{glass}, driven by high energy consumption and hydrogen prices. In 2050, its TAC decreases to 342 €/t_{glass}, narrowing the gap with NGOxyfur, but still exceeding those of Hybfur and ELfur. When combined with carbon capture (H2fur-CC), emissions are nearly eliminated, and TAC drops from 370 €/t_{glass} in 2025 to 300 €/t_{glass} in 2050. However, it remains less competitive than other decarbonisation options, highlighting that its long-term viability depends on substantial reductions in clean hydrogen prices.

Overall, while the NGfur-CC configuration is costly today, it may become viable under stricter environmental regulations. To meet net-zero targets and manage economic risks, a balanced strategy is essential, favouring hybrid configurations that reduce CO_2 emissions while ensuring cost stability. This approach is further strengthened by integrating CCS technologies, which offer flexibility to adapt to both high carbon prices and low electricity costs with minimal financial risk. Oxy-combustion with CCS is well-suited for scenarios with limited electrification potential. Full electrification remains sensitive to electricity prices, but the ELfur-CC option gains competitiveness with a decarbonised electricity grid. The long-term success of full electrification or hydrogen-based systems hinges on a significant decline in renewable energy prices. It is worth noting that these TAC results are based on the single-point price scenarios given in Table 5; the next section explores a broader price range to assess the feasibility of configurations under varying market conditions.

3.3 Multi-scenario mapping of configurations

The economic analysis identifies key cost drivers and the most cost-effective configurations under current and future energy scenarios. A multi-scenario mapping approach, using a deterministic parameter sweep, evaluates a wide range of electricity, NG, hydrogen, and CO_2 price combinations. This reveals the conditions under which each configuration is most economical, offering insights into their competitiveness and resilience across diverse future contexts. This mapping is illustrated by parallel coordinate plots given in Figures 11–15. Each line in the parallel coordinates plot represents an optimal solution for a specific combination of energy and emissions prices. The vertical axes show input parameters (electricity, hydrogen, NG, CO_2 prices), the selected technology, fuel and electricity demand, carbon capture deployment and resulting emissions. By following a line from left to right, one can trace how a particular price scenario leads to a specific configuration and its associated performance metrics.

According to Figure 11, NGfur remains the most competitive option under low to moderate carbon pricing, low NG prices, and moderate to high electricity prices. However, its competitiveness declines with rising emissions and NG prices, reflecting its sole reliance on NG and its high emissions intensity. In contrast, NGfur-CC becomes competitive only under extremely low NG and high electricity prices. It performs well in high carbon price scenarios (150–200 €/tCO_2), where CO_2 penalties justify the additional operational costs associated with carbon capture. It is only selected as optimal when full electrification becomes unfeasible, typically under high electricity price scenarios, while NG remains relatively cheap and CO_2 prices are elevated. This reflects that NGfur-CC depends on extreme boundary conditions to become economically viable, highlighting its limited robustness. It remains competitive only in scenarios where fuel switching or electrification is economically unfavourable. For both NGfur and NGfur-CC, carbon pricing and NG costs are the primary determining factors.

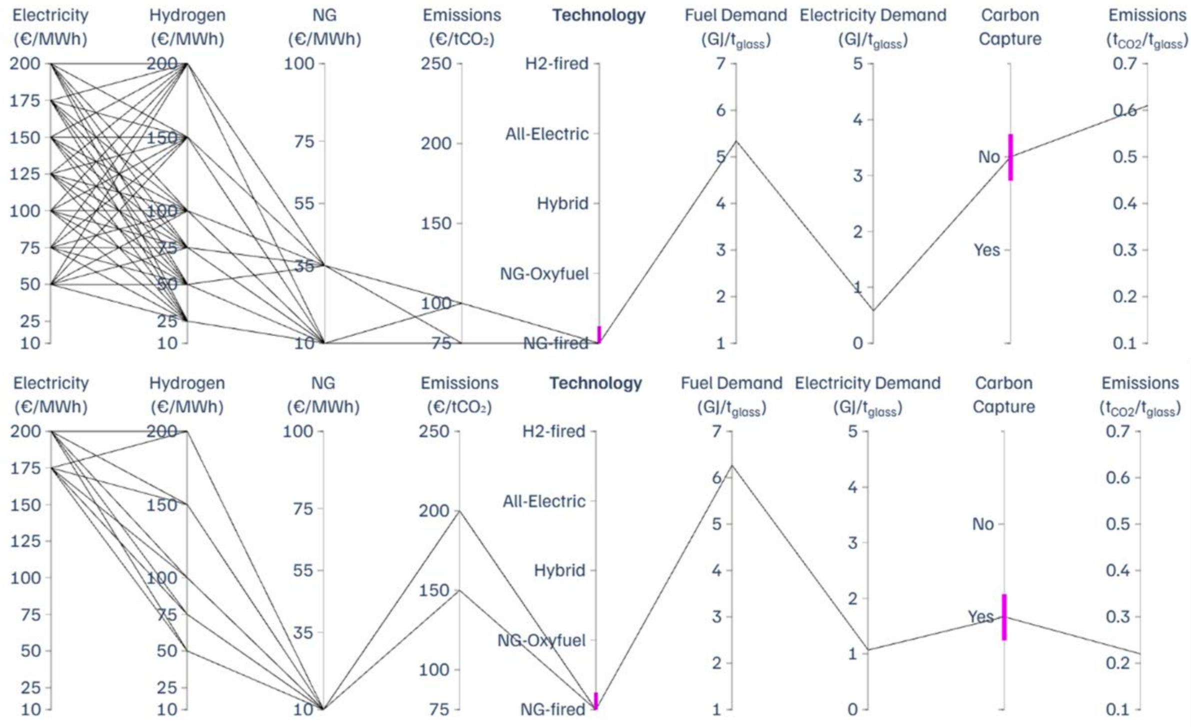

Figure 11. Parallel coordinates plot depicting the solution space of the NGfur configuration (top) and the NGfur-CC configuration (bottom) as a function of the commodities and CO_2 emissions prices.

Oxy-combustion-based configurations show a distinct sensitivity. NGOxyfur is selected under low to moderate carbon prices, moderate NG prices (35–55 €/MWh), and high electricity prices (>125 €/MWh), in scenarios where electrification options are uneconomical. Its moderate fuel and electricity use, combined with the lack of carbon capture, limit its suitability under strict carbon pricing. Compared to NGfur, it shows slightly more tolerance to NG price variations. Meanwhile, NGOxyfur-CC has a broader competitive range, viable under moderate to high carbon pricing (100–250 €/tCO_2), low to moderate NG prices (10–55 €/MWh) and electricity prices between 75–200 €/MWh. CCS integration mitigates emissions costs, enhancing resilience of NGOxyfur-CC even with a moderate increase in NG price. The solution spaces for NGOxyfur and NGOxyfur-CC configurations are shown in Figure 12.

Hybrid configurations, particularly the Hybfur-CC option, show remarkable versatility (Figure 13). Their balanced reliance on both NG and electricity allows them to adapt to a wide range of price scenarios. The moderate fuel demand and higher electricity use mean that both NG and electricity prices influence their competitiveness, but neither dominates entirely, by distributing exposure to volatile energy prices. Importantly, the Hybfur-CC configuration can maintain low emissions with a relatively modest increase in energy consumption, making it resilient in high CO_2 emissions price scenarios, without being overly sensitive to energy price fluctuations. This broad competitiveness suggests that the Hybfur-CC configuration effectively balances electrification and carbon capture, rendering it adaptable to a wider range of energy and emission price scenarios, proving its economic robustness.

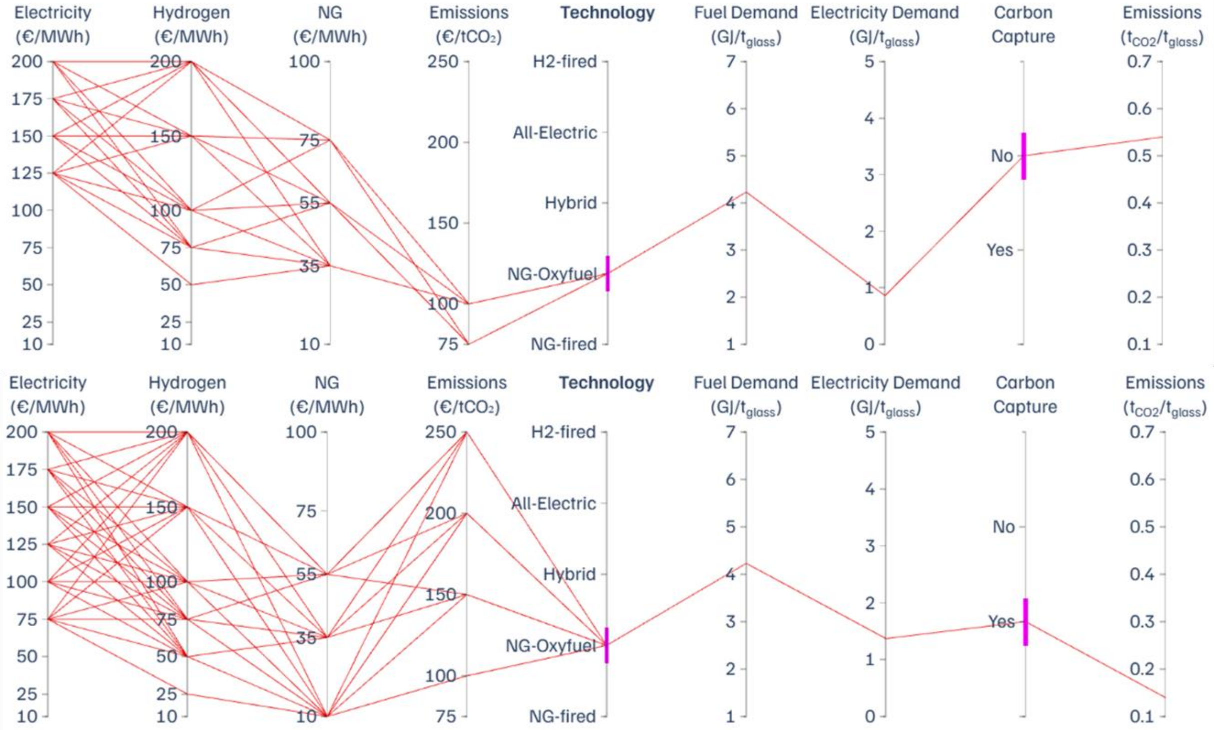

Figure 12. Parallel coordinates plot depicting solution space of NGOxyfur (top) and NGOxyfur-CC (bottom), as a function of the commodities and CO_2 emissions prices.

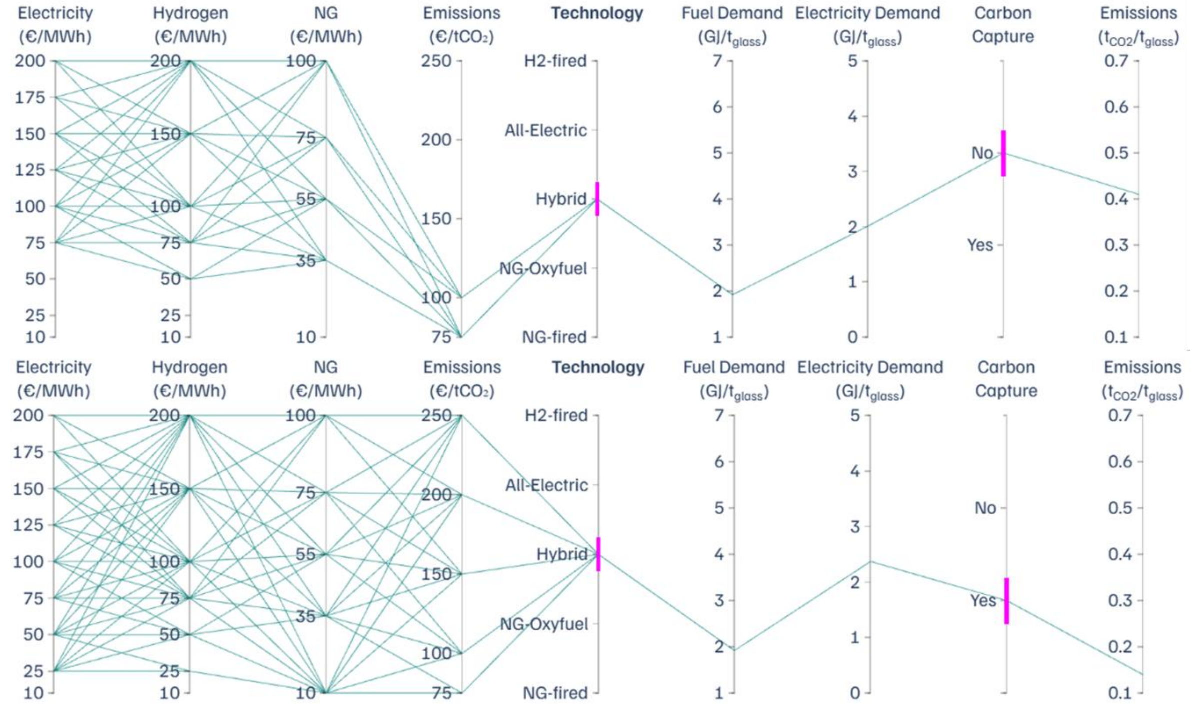

Figure 13. Parallel coordinates plot depicting solution space of Hybfur (top) and Hybfur-CC (bottom), as a function of the commodities and CO_2 emissions prices.

All-electric systems (ELfur and ELfur-CC) are, as expected, highly sensitive to electricity prices due to their complete reliance on electric input (Figure 14). The solution space for ELfur indicates that its viability is limited to scenarios with extremely high NG prices, very low emission costs, and electricity prices below 75–100 €/MWh. Any deviation, particularly an increase or decrease in electricity prices, quickly renders it less competitive, reflecting poor economic flexibility. The addition of carbon capture (ELfur-CC) improves its competitiveness by mitigating exposure to emissions costs. The combination of zero direct emissions through electrification and capture of process-related emissions makes ELfur-CC a promising option in highly decarbonised systems powered by cheap, low-carbon electricity. However, its feasibility remains strongly constrained by electricity prices, confirming that electricity cost is the dominant factor shaping the viability of all-electric configurations.

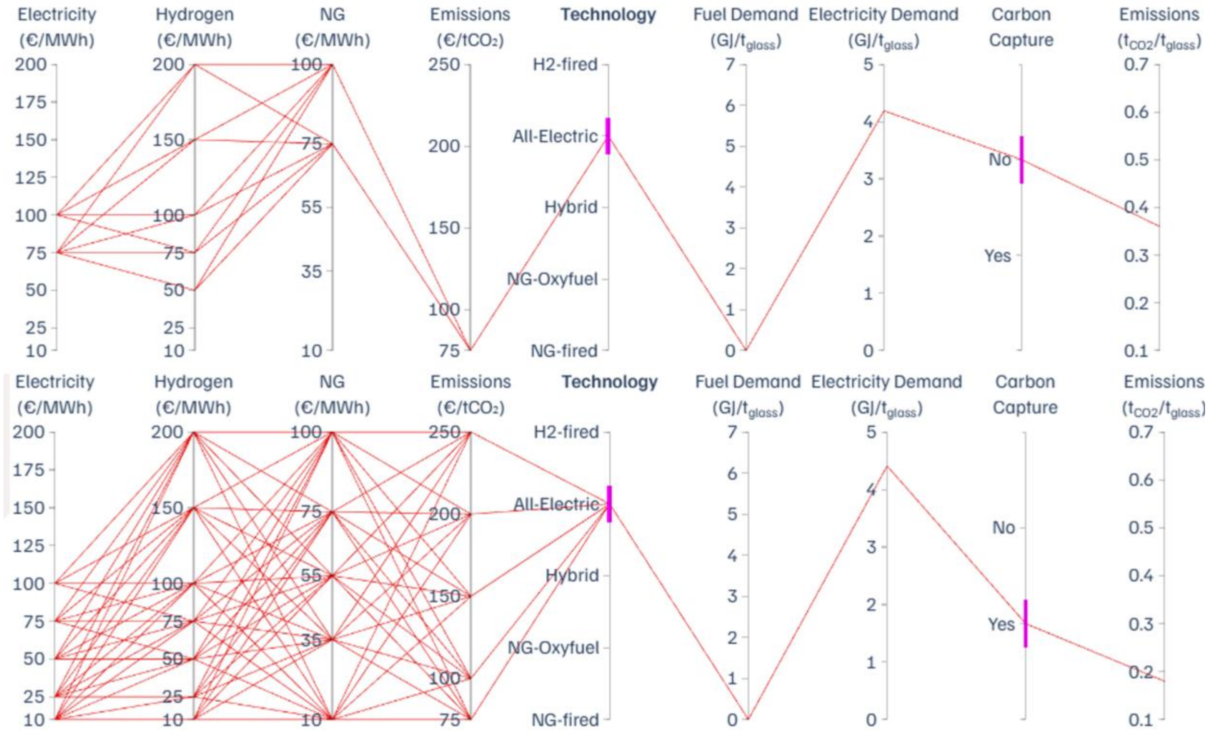

Figure 14. Parallel coordinates plot depicting solution space of ELfur (top) and ELfur-CC (bottom), as a function of the commodities and CO_2 emissions prices.

Hydrogen-based configurations (H2fur and H2fur-CC) are primarily influenced by hydrogen prices, given the role of hydrogen as the primary energy input. H2fur remains viable under conditions of low hydrogen prices (<75 €/MWh), moderate to high electricity prices (>50 €/MWh) and low carbon pricing (<150 €/tCO_2) (Figure 15). Although H2fur-CC incurs higher electricity demand due to carbon capture, its substantially reduced CO_2 emissions make it competitive under high carbon pricing. The key factor is that the emissions savings can compensate for the additional energy demand, but only when affordable green hydrogen is available. An interesting takeaway from Figures 14 and 15 is that if the prices of renewable electricity and hydrogen are in the same range, the optimiser will choose electrification as the preferred solution. Hence, for H2fur configurations to be feasible, hydrogen prices must be comparatively lower than electricity prices.

The occurrence of each configuration in the solution space reflects a complex interplay of energy demand, emissions, and economic viability. High energy demand increases sensitivity to price fluctuations, while carbon-intensive systems are penalised under rising CO_2 prices. Carbon capture broadens the solution space, enhancing competitiveness in high-emission-cost scenarios. Among all options, Hybfur and Hybfur-CC configurations emerge as the most robust and adaptable options, as they appear for a wide range of prices, followed by NGOxyfur (-CC). ELfur-CC performs well in low-carbon electricity scenarios, while hydrogen-based systems offer long-term potential, contingent on the availability of low-cost hydrogen.

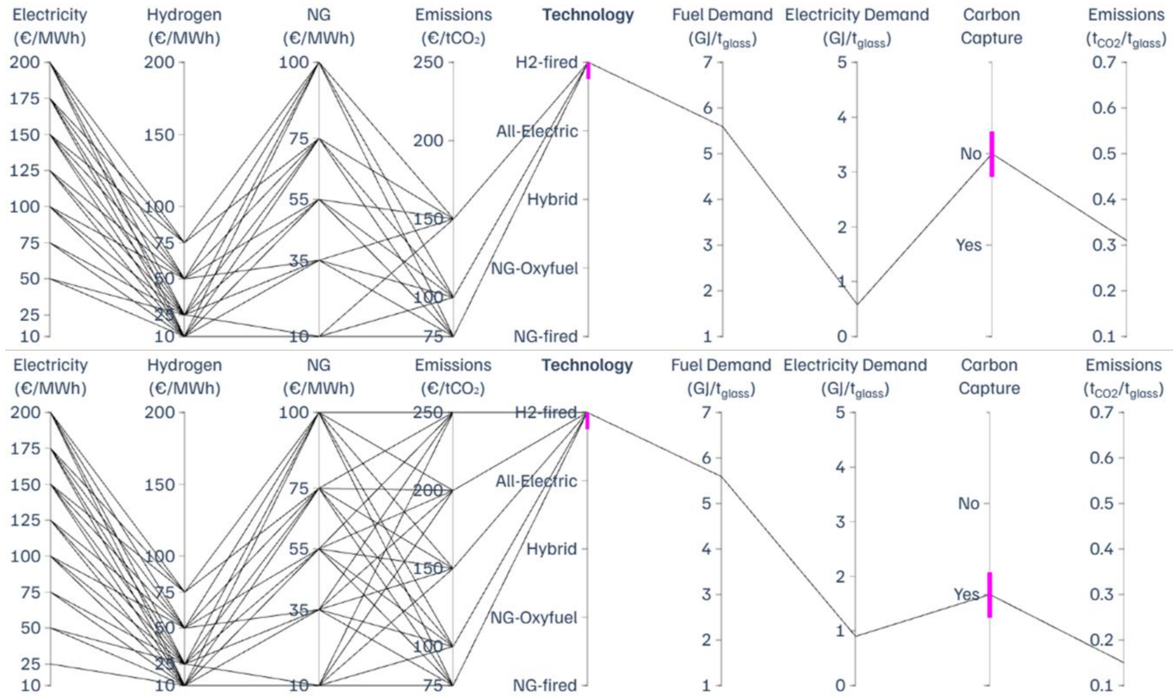

Figure 15. Parallel coordinates plot depicting solution space of H2fur (top) and H2fur-CC (bottom), as a function of the commodities and CO_2 emissions prices.

3.4 Uncertainty analysis

While multi-scenario mapping identifies optimal conditions, it does not reflect uncertainties in future energy and CO_2 prices. This section addresses this gap by integrating probabilistic scenario inputs through PCE, enabling a stochastic evaluation of each configuration's cost-effectiveness. TAC distributions are generated for each configuration and target year, based on input price distributions (given in Figures S8 and S9). Figure 16 presents the resulting cumulative distribution functions (CDFs), where each curve shows the probability that the TAC of a configuration remains below a certain value across a wide range of price scenarios. Curves positioned further to the left represent more cost-effective options, while steeper slopes indicate higher cost stability (i.e., predictable performance). In contrast, flatter curves suggest greater sensitivity to price fluctuations. Comparing curves across 2030, 2040, and 2050 highlights how economic robustness evolves over time.

3.4.1 Stochastic performance of technologies

Figure 16 illustrates the stochastic TAC performance across future energy scenarios. In 2030 (moderate energy and CO_2 prices, low uncertainty), NG-based configurations remain cost-optimal, with small differences in TAC. Hybfur (with and without CC) emerges as the most stable option, followed by NGOxyfur, indicated by steep CDF profiles showing low TAC variance. In contrast, all-electric and hydrogen-based configurations exhibit higher TAC values and significant cost uncertainty, reflecting their sensitivity to volatile energy prices.

By 2040 (lower energy prices, higher CO_2 prices, increased uncertainty), alternative fuel configurations gain competitiveness but remain highly uncertain, with flatter CDF curves. For example, at a TAC threshold of 280 €/t_{glass}, H2fur-CC surpasses NGOxyfur-CC in the probability of being lower. However, at higher TAC thresholds, NGOxyfur-CC remains preferred due to greater cost stability; at 300 €/t_{glass}, NGOxyfur-CC has a 70% probability of staying below the threshold, to 55% for H2fur-CC.

In 2050 (i.e., with further CO_2 price increases, lower energy prices and heightened uncertainty), configurations integrating carbon capture achieve the lowest TAC, driven by rising CO_2 penalties. However, their flatter CDFs reflect higher uncertainty compared to alternatives without carbon capture. For example, the ELfur-CC configuration becomes more competitive at lower TAC thresholds, although its relatively flatter CDF indicates greater cost variability than NGfur. Notably, Hybfur-CC demonstrates both low TAC values and steeper CDF curves, highlighting its superior stability and adaptability in an uncertain energy landscape, owing to its balanced integration of partial electrification and fuel flexibility.

Overall, the stochastic analysis shows that NG-based configurations remain cost-optimal in 2030, but they lose competitiveness with market uncertainties. Hybfur and NGOxyfur configurations offer greater resilience. By 2040, lower energy and higher CO_2 prices boost alternative fuels, although the economic performance of hydrogen and electrified systems remains uncertain, holding lower TAC. In 2050, technologies incorporating carbon capture achieve low TAC values, but at the expense of higher uncertainty; whereas Hybfur-CC configuration remains the most stable and adaptable option, balancing both partial electrification and fuel flexibility.

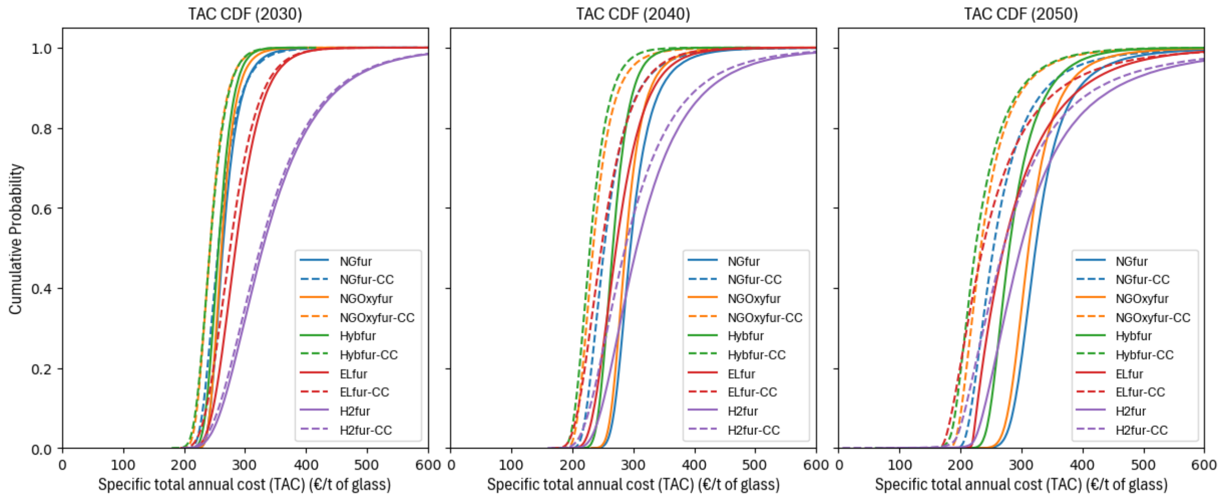

Figure 16. Cumulative distribution functions (CDFs) of the TAC for all the studied configurations over time.

3.4.2 Probability of Achieving a Competitive TAC

To further assess uncertainty in the economic performance of the configurations, a TAC threshold of 300 €/t_{glass} is selected from the CDFs for 2030, 2040 and 2050. Since the 2025 TAC for the base case (NGfur) was 237 €/t_{glass} (cf. Section 3.2.3), a moderate increase over time makes 300 €/t_{glass} a suitable benchmark for evaluating configuration under evolving energy and emissions scenarios (Figure 17).

In 2030, NGfur, NGOxyfur and Hybfur configurations show high probabilities (>90%) of maintaining TAC below 300 €/t_{glass}, reaffirming the near-term cost-effectiveness of NG-based options. Conversely, ELfur and H2fur configurations show significantly lower probabilities, reflecting their economic disadvantage under moderate carbon and energy prices. By 2040 and 2050, as carbon prices rise and energy market uncertainty increases, the probability for NG-based configurations declines sharply, making them riskier. Meanwhile, ELfur and H2fur gain competitiveness, achieving higher probabilities of remaining below the threshold in 2050. Hybfur, despite a probability decline, remains the most stable non-CC option, with a much less pronounced decrease than NGfur and NGOxyfur, highlighting its resilience in increasingly uncertain markets. Among carbon capture configurations, Hybfur-CC and NGOxyfur-CC remain the most reliable, maintaining a 98% probability in 2030, slightly decreasing to 90% by 2050. NGfur-CC shows a sharper decline, dropping from 90% in 2030 to 79% in 2050, reflecting its increasing exposure to carbon cost risks. ELfur-CC improves from 73% in 2030 to 86% in 2040, before slightly declining to 79% in 2050 due to electricity price uncertainty.

These findings highlight that if future policies enforce high carbon prices, continued reliance on NGfur will lead to significant cost volatility and elevated TAC risks. In contrast, electrification-based solutions, particularly Hybfur, offer greater stability and lower TAC exposure. If CCS becomes essential, NGfur-CC faces higher financial risks compared to NGOxyfur-CC and Hybfur-CC, which show lower uncertainty and reduced cost exposure. While ELfur-CC and H2fur-CC serve as viable low-emission alternatives, their greater cost variability makes them less predictable than other CCS-based solutions. Overall, these insights emphasise the importance of fuel flexibility and risk-mitigation strategies in selecting a cost-effective, future-proof decarbonisation pathway for the glass industry.

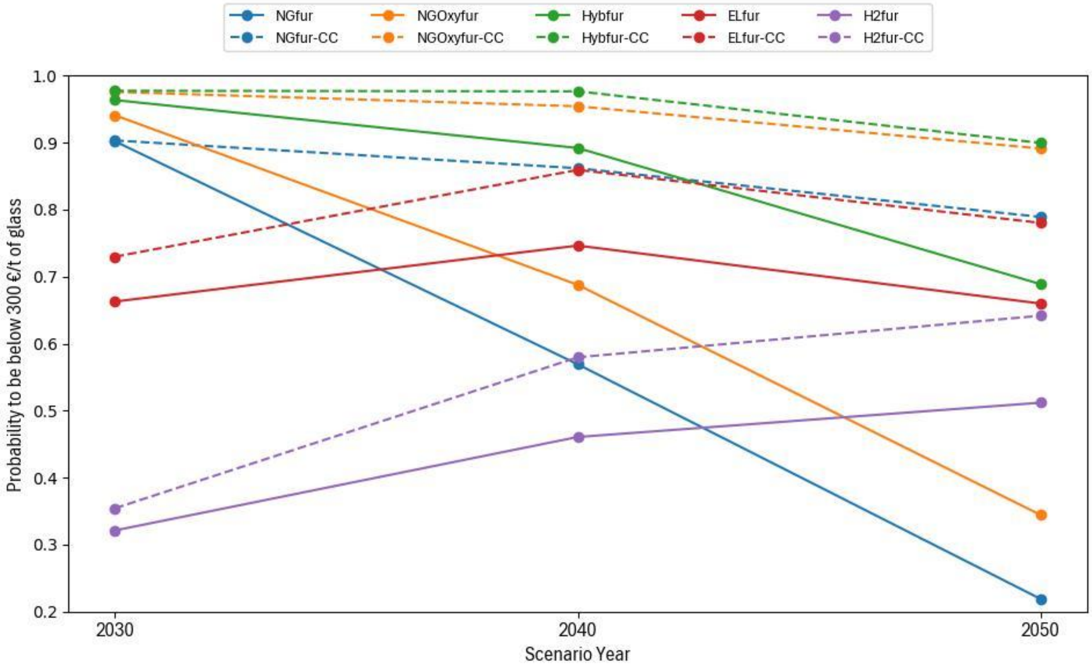

Figure 17. Probability of each configuration achieving a TAC of 300 €/t_{glass} or lower for each target year.

4 Conclusions

This study presents a comprehensive techno-economic assessment of decarbonisation pathways for the glass industry, integrating energy efficiency, fuel switching, electrification and CCS. Moreover, a combination of multi-scenario mapping and uncertainty assessment was employed to evaluate the competitiveness and economic feasibility of various configurations under evolving energy markets and CO_2 emission prices.

The analysis begins with a detailed carbon footprint assessment of each configuration, accounting for both direct and indirect emissions. Results show that NGfur (base case) systems have the highest emissions in the 2025 scenario, while carbon capture (NGfur-CC) can reduce net emissions by up to 74%. Hybrid configurations emerge as an effective transitional pathway, achieving significant emission reductions through partial electrification and CCS integration. Electrification and hydrogen eliminate combustion-related emissions and offer maximum emission reductions when coupled with renewable electricity or green hydrogen.

The energy consumption analysis shows that the NGOxyfur configuration enhances thermal efficiency, while Hybfur reduces NG use and emissions by 33% compared to the base case (NGfur). ELfur, based on full electrification, eliminates fossil fuel dependency but relies entirely on green electricity. Carbon capture reduces emissions but increases total energy demand by 5–22% to achieve 50–74% emission reductions. NGfur-CC holds the highest energy demand, while Hybfur and Hybfur-CC offer the best balance between efficiency and emissions reduction.

The TAC analysis shows that while NGfur remains the least-cost option in 2025 (237 €/t_{glass}), its TAC rises by 57% in 2050, making NGfur-CC more attractive. NGOxyfur-CC offers a 10% lower TAC than NGfur-CC in 2050, benefiting from improved efficiency and lower emissions. Hybfur and Hybfur-CC configurations emerge as the most resilient pathways, with Hybfur-CC achieving a 17% lower TAC than NGfur-CC in 2050 while offering superior stability under varying market conditions. ELfur-CC also gains competitiveness, reducing its TAC by 19% from 2025 to 2050, reflecting the advantages of renewable electricity. In contrast, despite achieving significant emissions reduction, H2fur-CC remains costlier, emphasising the need for substantial declines in green hydrogen prices. Ultimately, hybrid configurations provide the most flexible and stable route toward net-zero glass production, offering the best balance between emissions reduction, cost stability and energy market adaptability.

A multi-scenario mapping shows that emissions and energy prices heavily influence the selection of the optimal configuration. NGfur setup remains viable at low carbon (75–100 €/tCO_2) and NG (10–35 €/MWh) prices, while NGfur-CC becomes competitive only at extremely low NG and high CO_2 prices, exhibiting its limited robustness. NGOxyfur-CC configuration, with lower energy demand and better capture efficiency, remains viable across a broader range of scenarios. Hybfur and Hybfur-CC configurations offer the highest adaptability, making hybrid configurations the most robust choice under varying market conditions. ELfur-CC configuration gains competitiveness with low electricity (<100 €/MWh) and high CO_2 prices, but remains cost-sensitive. H2fur-CC configuration requires hydrogen prices below 75 €/MWh and is relatively cheaper than renewable electricity, therefore relying on major cost reductions in energy vectors.

Finally, an uncertainty analysis showed that NG-based technologies remain cost-effective in 2030, but lose competitiveness as carbon prices rise. Hybfur and NGOxyfur configurations offer greater resilience, with the Hybfur-CC configuration emerging as the most stable due to partial electrification and emission reductions. By 2040, alternative fuels gain traction, although hydrogen and electrification pathways remain uncertain. In the 2050 scenario, configurations integrating carbon capture achieve lower TAC, but with higher uncertainty, while Hybfur-CC configuration balances cost and predictability among carbon capture options. Hybfur-CC and NGOxyfur-CC solutions are the most reliable, while the NGfur-CC configuration faces higher financial risks.

In summary, the decarbonisation potential of flat glass production depends heavily on energy and carbon pricing. Hybrid configurations emerge as the most cost-effective and resilient solutions, balancing emissions reduction, efficiency and cost stability, while offering more predictability. Oxy-combustion options remain a strong alternative only when electrification options are rendered infeasible. Fully electrified pathways depend entirely on low-cost renewable electricity, while hydrogen-based furnaces offer limited potential unless hydrogen prices drop significantly. Although carbon capture may face near-term economic challenges, declining renewable costs and moderate increases in carbon cost could make Hybfur-CC and NGOxyfur-CC configurations more cost-competitive. The analysis highlights the Hybfur (-CC) configuration as the most adaptable and strategically viable pathway, ensuring economic stability in an evolving energy landscape.

The future of glass industry decarbonisation will hinge on scaling CCS infrastructure and decreasing renewable electricity costs. Focus on flexible decarbonisation strategies, such as partial electrification, is essential for ensuring cost stability and emissions reductions. The industry must focus on scalable, adaptable technologies, while policymakers should create regulatory frameworks that promote low-carbon electricity and CCS deployment. This study focused on only two capture options (CC-MEA and CC-CPU), excluding other promising methods like membranes or solid sorbents, which should be explored in future research. Moreover, the analysis assumes full access to electricity, hydrogen, NG, and CO_2 networks, excluding infrastructure connection costs, except for CO_2 transport. Fixed OPEX, owner's costs, and material factors were also omitted, assuming similar values across configurations, which may not hold in practice and affect absolute cost accuracy. Results should therefore be interpreted as relative indicators of cost competitiveness. Future research should also explore on-site renewables, CO_2 utilisation, circular economy strategies like increased cullet recycling and scenario-based policy modelling to evaluate carbon cost and regulations. A multi-sector integration approach involving industrial symbiosis can also be explored for a cost-effective net-zero transition in the glass industry.

Finally, this study illustrates the effectiveness of the process systems engineering (PSE) tools for assessing decarbonisation options in the energy-intensive industries. The integration of energy, emissions, and cost calculations into an equation-oriented modelling framework enables a holistic evaluation and comparison of multiple configurations. Notably, the incorporation of uncertainty analysis, which captures the impact of fluctuating energy and CO_2 prices, allowed the identification of robust solutions. While the current approach demonstrates strong sectoral applicability, broader adoption across other industries could benefit from improved interoperability, integration of detailed LCA and tighter integration with uncertainty quantification and surrogate modelling techniques. These enhancements could increase the accessibility of such methods to several industrial sectors.

Acknowledgements

The authors would like to thank the support of the Energy Transition Fund project TRILATE, organised by the FPS Economy, Belgium. Additionally, D.F-O thanks the Swiss Federal Office of Energy for the support in the context of the project "Continuous Training Program: Process Engineering for Decarbonisation of the Swiss Industry". D.C. also acknowledges funding from the Fonds de la Recherche Scientifique - FNRS [CR 40016260]. R.M. additionally thanks the FRS-FNRS for a FRIA scholarship. The authors would also like to express gratitude to AGC Glass Europe (Belgium) for their valuable feedback.

References

Air Liquide, 2020. Air Liquide invests in the first world-scale oxygen production plant fit to accommodate renewable energy in the grid. https://www.airliquide.com/group/press-releases-news/2020-07-23/air-liquide-invests-first-world-scale-oxygen-production-plant-fit-accommodate-renewable-energy-grid (accessed 5.1.25).

B. Fleischmann, 2018. Neuer Ansatz zur Bilanzierung des Energieeinsatzes bei der GLasherstellung und der Versuch der geschlossenen Darstellung von Kennzahlen zum Energieverbrauch aus der Produktionstechnik und aus statistischen (Wirtschafts-) Daten. Deutschen Glastechnischen Gesellschaft (DGG) 17, 11–22.

Barlow, H., Shahi, S.M.S., Loughrey, M., 2023. State of the art: CCS Technologies 2023. Brussels.

Barón, C., Perpiñán, J., Bailera, M., Peña, B., 2023. Techno-economic assessment of glassmaking decarbonization through integration of calcium looping carbon capture and power-to-gas technologies. Sustain Prod Consum 41, 121–133. https://doi.org/https://doi.org/10.1016/j.spc.2023.07.029

Bataille, C., Åhman, M., Neuhoff, K., Nilsson, L.J., Fischedick, M., Lechtenböhmer, S., Solano-Rodriquez, B., Denis-Ryan, A., Stiebert, S., Waisman, H., 2018. A review of technology and policy deep decarbonization pathway options for making energy-intensive industry production consistent with the Paris Agreement. J Clean Prod 187, 960–973.

Blackburn, A., 2016. Flat Glass Manufacturers Expand into Developing Areas. https://blog.marketresearch.com/flat-glass-manufacturers-expand-into-developing-areas (accessed 1.23.25).

British Glass, 2021. Glass sector Net zero strategy 2050. Sheffield.

Business Analytiq, 2024. Blue hydrogen price index. https://businessanalytiq.com/procurementanalytics/index/blue-hydrogen-price-index/ (accessed 1.23.25).

Cervo, H., Ferrasse, J.-H., Descales, B., Van Eetvelde, G., 2020. Blueprint: A methodology facilitating data exchanges to enhance the detection of industrial symbiosis opportunities – application to a refinery. Chem Eng Sci 211, 115254. https://doi.org/https://doi.org/10.1016/j.ces.2019.115254

Climact, 2021. Scenarios for a climate neutral Belgium by 2050. Brussels.

Colangelo, S., 2024. Reducing the environmental footprint of glass manufacturing. Int J Appl Glass Sci 15, 350–366. https://doi.org/10.1111/ijag.16674

CoolProp, 2023. Welcome to CoolProp — CoolProp 6.6.0 documentation. http://www.coolprop.org (accessed 2.10.25).

Coppitters, D., De Paepe, W., Contino, F., 2020. Robust design optimization and stochastic performance analysis of a grid-connected photovoltaic system with battery storage and hydrogen storage. Energy 213, 118798. https://doi.org/https://doi.org/10.1016/j.energy.2020.118798

Coppitters, D., Tsirikoglou, P., De Paepe, W., Kyprianidis, K., Kalfas, A., Contino, F., 2022. RHEIA: Robust design optimization of renewable Hydrogen and dErIved energy cArrier systems. The Journal of Open Source Software 7, 4370. https://doi.org/10.21105/joss.04370

Costa, A., Coppitters, D., Dubois, L., Contino, F., Thomas, D., De Weireld, G., 2024. Energy, exergy, economic and environmental (4E) analysis of a cryogenic carbon purification unit with membrane for oxyfuel cement plant flue gas. Appl Energy 357, 122431. https://doi.org/https://doi.org/10.1016/j.apenergy.2023.122431

DG Energy, 2024a. Quarterly report on European electricity markets. Brussels.

DG Energy, 2024b. Quarterly report on European Gas Market. Brussels.

DG-Energy European Commission, 2015. Study on actual GHG data for Diesel, Petrol, kerosene and Natural Gas. Brussels.

Ecofys, Fraunhoffer, Öko-Institut, 2012. Methodology for the free allocation of emission allowances in the EU ETS post 2012: Sector report for the glass industry.

EEA, 2024. Greenhouse gas emission intensity of electricity generation in Europe. Copenhagen.

ELIA, 2017. Electricity Scenarios for Belgium Towards 2050: ELIA's Quantified study on the energy transition in 2030 and 2040. Brussels.

EnergyVille, 2023. PATHS 2050 - Scenarios towards a carbon-neutral Belgium by 2050. Genk.

ENTSO, 2024. Ten-year network development plans (TYNDP) 2024: Scenario Report. Brussels.

ENTSO, 2022. Ten-year network development plans (TYNDP) 2022: Scenario Report. Brussels.

ETS, 2023a. EU ETS dataviewer. https://www.eea.europa.eu/en/analysis/maps-and-charts/emissions-trading-viewer-1-dashboards (accessed 12.29.24).

ETS, 2023b. EU ETS Verified Emissions for 2023. https://climate.ec.europa.eu/document/download/ebb2c20e-8737-4a73-b6ba-a4b7e78ecc01_en?filename=verified_emissions_2023_en_1.xlsx

European Commission, 2023. Consequences of climate change. https://climate.ec.europa.eu/climate-change/consequences-climate-change_en (accessed 12.28.24).

European Commission, 2021. Fit for 55': delivering the EU's 2030 Climate Target on the way to climate neutrality. Brussels.

European Commission, 2018. A Clean Planet for all: A European strategic long-term vision for a prosperous, modern, competitive and climate neutral economy. Brussels.

Flórez-Orrego, D., Dardor, D., Reginal, G., Maréchal, F., 2023. A systemic study for enhanced waste heat recovery and renewable energy integration towards decarbonizing the aluminium industry, in: Proceeding of the 36th International Conference on Efficiency, Cost, Optimisation, Simulation and Environmental Impact of Energy Systems - ECOS 2023.

Flórez-Orrego, D., Ribeiro Domingos, M.E.G., Maréchal, F., 2022. A systematic framework for the multi-time integration of industrial complexes and urban systems, in: 7th International Conference on Contemporary Problems of Thermal Engineering - CPOTE 2022. Warsaw, Poland.

Fluxys, 2022. Carbon Specification Proposal. https://www.fluxys.com/-/media/project/fluxys/public/corporate/fluxyscom/documents/energy-transition/co2/2022-03-30---carbon-specification-proposal---march-22.pdf (accessed 1.6.25).

Fluxys, n.d. CO_2, much more than a greenhouse gas. https://www.fluxys.com/en/co2#/ (accessed 2.12.25).

Frischknecht, R., Krebs, L., 2021. Environmental life cycle assessment of electricity from PV systems - Fact Sheet 2021.

Fujita, S.K., 2021. Commercial, industrial, and institutional discount rate estimation for efficiency standards analysis: Sector-level data 1998-2020.

Fuller, A., García, P.G., Hulme, R., Ireson, R., 2022. Alternative Fuel Switching Technologies for the Glass Sector: Phase 3. London.

Gardarsdottir, S.O., De Lena, E., Romano, M., Roussanaly, S., Voldsund, M., Pérez-Calvo, J.F., Berstad, D., Fu, C., Anantharaman, R., Sutter, D., Gazzani, M., Mazzotti, M., Cinti, G., 2019. Comparison of technologies for CO_2 capture from cement production—Part 2: Cost analysis. Energies (Basel) 12. https://doi.org/10.3390/en12030542

Gefland, A.E., Smith, A.F.M., 1990. Sampling-Based Approaches to Calculating Marginal Densities. J Am Stat Assoc 85, 398–409. https://doi.org/https://doi.org/10.2307/2289776

Glass for Europe, 2020a. Flat Glass in Climate-neutral Europe: Triggering a Virtuous Cycle of Decarbonisation. Etterbeek.

Glass for Europe, 2020b. ‘Hot hold’ operations in the flat glass sector. https://glassforeurope.com/hot-hold-operations-in-the-flat-glass-sector/ (accessed 4.27.25).

Griffin, P.W., Hammond, G.P., McKenna, R.C., 2021. Industrial energy use and decarbonisation in the glass sector: A UK perspective. Advances in Applied Energy 3, 100037. https://doi.org/https://doi.org/10.1016/j.adapen.2021.100037

Hoffman, M.D., Gelman, A., 2014. The No-U-Turn Sampler: Adaptively Setting Path Lengths in Hamiltonian Monte Carlo. Journal of Machine Learning Research 15, 1593–1623.

IEA, 2023. Comparison of the emissions intensity of different hydrogen production routes, 2021.. https://www.iea.org/data-and-statistics/charts/comparison-of-the-emissions-intensity-of-different-hydrogen-production-routes-2021 (accessed 1.12.25).

Joint Research Centre, 2013. Best available techniques (BAT) reference document for the manufacture of glass – Industrial emissions Directive 2010/75/EU: integrated pollution prevention and control. Publications Office. https://doi.org/doi/10.2791/70161

Kapoor, A., Schatz, C., 1997. Process for recovering waste gases of a glass melting furnace. EP0761287A2.

Kim, S., Léonard, G., 2025. CO_2 capture technologies and shortcut cost correlations for different inlet CO_2 concentrations and flow rates. part 1: Chemical absorption. International Journal of Greenhouse Gas Control 145, 104391. https://doi.org/https://doi.org/10.1016/j.ijggc.2025.104391

Kobayashi, H., 2004. Advances in Oxy-Fuel Fired Glass Melting Technology. Danbury, CT, USA.

Li, Z., He, X., Wang, Y., Zhang, B., He, H., 2014. Design of a flat glass furnace waste heat power generation system. Appl Therm Eng 63, 290–296. https://doi.org/10.1016/j.applthermaleng.2013.10.038

Lyons, S., Durusut, E., Moore, I., 2018. Industrial Fuel Switching - Market Engagement Study. Cambridge.

Marelli, S., Sudret, B., 2014. UQLab: A Framework for Uncertainty Quantification in Matlab. https://doi.org/10.1061/9780784413609.257

Morris, G., 2020. Will hydrogen be the new energy carrier for glassmaking?. https://www.glass-international.com/features/will-hydrogen-be-the-new-energy-carrier-for-glassmaking (accessed 1.22.25).

Napp, T.A., Gambhir, A., Hills, T.P., Florin, N., Fennell, P.S., 2014. A review of the technologies, economics and policy instruments for decarbonising energy-intensive manufacturing industries. Renewable and Sustainable Energy Reviews 30, 616–640. https://doi.org/https://doi.org/10.1016/j.rser.2013.10.036

Papadogeorgos, I., Schure, K.. M., 2019. Decarbonisation options for the dutch container and tableware glass industry. PBL Netherlands Environmental Assessment Agency, The Hague.

Rademaker, K., Marsidi, M., 2019. Decarbonisation options for the Dutch sugar industry. The Hague.

Roussanaly, S., Berghout, N., Fout, T., Garcia, M., Gardarsdottir, S., Nazir, S.M., Ramirez, A., Rubin, E.S., 2021. Towards improved cost evaluation of Carbon Capture and Storage from industry. International Journal of Greenhouse Gas Control 106, 103263. https://doi.org/https://doi.org/10.1016/j.ijggc.2021.103263

Salman, M., Beguin, B., Nyssen, T., Léonard, G., 2024. Techno-economic analysis of AMP/PZ solvent for CO2 capture in a biomass CHP plant: towards net negative emissions. Front Energy Res 12. https://doi.org/10.3389/fenrg.2024.1325212

Schlömer, S., Bruckner, T., Fulton, L., Hertwich, E., 2014. Annex III: Technology-specific cost and performance parameters. In: Climate Change 2014: Contribution of Working Group III to the Fifth Assessment Report of the Intergovernmental Panel on Climate Change, Climate Change 2014: Mitigation of Climate Change.

Shah, M.M., 2011. 11 - Carbon dioxide (CO2) compression and purification technology for oxy-fuel combustion, in: Zheng, L. (Ed.), Oxy-Fuel Combustion for Power Generation and Carbon Dioxide (CO2) Capture. Woodhead Publishing, pp. 228–255. https://doi.org/https://doi.org/10.1533/9780857090980.2.228

Statista, 2024. Daily European Union Emission Trading System (EU-ETS) carbon pricing from 2022 to 2024. https://www.statista.com/statistics/1322214/carbon-prices-european-union-emission-trading-scheme/ (accessed 1.20.25).

Turton, R., Shaeiwitz, J.A., Whiting, W.B., Bhattacharyya, D., 2018. Analysis, Synthesis, and Design of Chemical Processes, 5th ed, Prentice-Hall international series in engineering. Prentice Hall.

Wright, S.A., Anderson, M., 2017. Workshop on New Cross-cutting Technologies for Nuclear Power Plants: Session 2: Supercritical CO2 cycle for advanced NPPs.

Zier, M., Pflugradt, N., Stenzel, P., Kotzur, L., Stolten, D., 2023. Industrial decarbonization pathways: The example of the German glass industry. Energy Conversion and Management: X 17, 100336. https://doi.org/https://doi.org/10.1016/j.ecmx.2022.100336

Zier, M., Stenzel, P., Kotzur, L., Stolten, D., 2021. A review of decarbonization options for the glass industry. Energy Conversion and Management: X 10, 100083. https://doi.org/https://doi.org/10.1016/j.ecmx.2021.100083